BOREAL ENVIRONMENT RESEARCH 19 (suppl. B): 153–181 © 2014
ISSN 1239-6095 (print) ISSN 1797-2469 (online) Helsinki 30 September 2014

Airborne measurements of aerosols and carbon dioxide during a prescribed fire experiment at a boreal forest site

Aki Virkkula[1),2)], Toivo Pohja[3)], Pasi P. Aalto[1)], Petri Keronen[1)], Siegfried Schobesberger[1)], Craig B. Clements[4)], Tuukka Petäjä[1)], Juha Nikmo[2)] and Markku Kulmala[1)]

[1)] *Department of Physics, P.O. Box 64, FI-00014 University of Helsinki, Finland*
[2)] *Finnish Meteorological Institute, Research and Development, P.O. Box 503, FI-00101 Helsinki, Finland*
[3)] *Hyytiälä Forestry Field Station, University of Helsinki, FI-35500 Korkeakoski, Finland*
[4)] *Department of Meteorology and Climate Science, San José State University, San José, CA 95192, USA*

Received 12 Dec. 2013, final version received 28 May 2014, accepted 28 May 2014

Virkkula, A., Pohja, T., Aalto, P. P., Keronen, P., Schobesberger, S., Clements, C. B., Petäjä, T., Nikmo, J. & Kulmala, M. 2014: Airborne measurements of aerosols and carbon dioxide during a prescribed fire experiment at a boreal forest site. *Boreal Env. Res.* 19 (suppl. B): 153–181.

During a prescribed fire experiment, CO_2 and particle number concentrations, light scattering and absorption coefficients were measured from a Cessna 172 airplane. Peak number concentrations were $(3 \pm 1) \times 10^6$ cm^{-3} and they decreased faster than what can be explained by coagulation alone. The single-scattering albedo of particles grew from the values of 0.4 ± 0.1 closest to the emissions to the values of 0.8 ± 0.1 at the distance of 400 m from the emissions. The mean Ångström exponent of absorption, 1.70 ± 0.24, is in line with the published spectral absorption values of wood-smoke aerosol. The estimated emission factors were 1600 ± 1020, 5.9 ± 6.3 and 1.4 ± 1.0 g kg^{-1} (dry biomass), for CO_2, particulate organic matter and black carbon (BC), respectively, and $(4.8 \pm 2.9) \times 10^{15}$ particles per kg (dry biomass) for the particle number. The BC emission factor may be overestimated by a factor of about 1.6 ± 0.2 due to condensation of organics on the filter of the absorption photometer. During the smoldering phase, there were clear indications of new particle formation.

Introduction

Wildfire emissions have significant climatic effects. Greenhouse gases and black carbon emitted from the fires heat the atmosphere but the emitted particles also cool the atmosphere depending on their size and chemical composition and the underlying surface (e.g. Carrico *et al*. 2010, Chand *et al*. 2009). The smoke from wildfires can be transported over long distances from the boreal forest areas to the Arctic, where it has significant climatic effects both in the atmosphere and on snow and ice surfaces (e.g. Goldammer *et al*. 1996, Randerson *et al*. 2006, Law and Stohl 2007, Quinn *et al*. 2008, AMAP 2011). Image analyses of wildfires observed from space by satellites provide information on the area burned (e.g. Flannigan and Haar 1986, Lentile *et al*. 2006, French *et al*. 2008, van der Werf *et al*. 2010), but not on the amount of fuel

Editor in charge of this article: Veli-Matti Kerminen

consumed or the amount and composition of the smoke. In order to estimate that, the emission factors, defined as the amount of emitted aerosol or trace gases per mass unit of burned biomass, are needed (e.g. Andreae and Merlet 2001, Reid *et al*. 2005a, 2005b, Janhäll *et al*. 2010, Akagi *et al*. 2011, Simpson *et al*. 2011, Yokelson *et al*. 2013). In wildfires, biomass fuels are consumed both by flaming combustion, in which most of the emissions are lofted vertically in a convection column associated with the flaming front, and by smoldering combustion. The residual smoldering combustion (RSC) is biomass combustion that produces emissions that are not lofted by strong fire-induced convection (e.g. Wade and Lunsford 1989, Bertschi *et al*. 2003, Akagi *et al*. 2011). RSC emissions can be produced for up to several weeks after the crossing of a flame front and they are potentially a globally significant source of emissions to the troposphere (e.g. Bertschi *et al*. 2003, Akagi *et al*. 2011, Burling *et al*. 2011).

Detailed measurements of gas and aerosol emissions are easier to arrange in prescribed fires of forest than in active wildfires: in the latter the fire may be too large and uncontrolled and in a difficult location for taking measurements near it. For the past few decades, emissions from prescribed fires have often been measured using aircraft. For example, Stith *et al*. (1981) measured particle size distributions, light scattering coefficient and ozone concentrations above three prescribed burns in the northwestern USA, Mazurek *et al*. (1991) used a helicopter platform to take filter samples from a boreal forest prescribed burn in Ontario, Canada. Burling *et al*. (2011) measured emission factors for several trace gas species and particulate matter from 14 prescribed fires in the southwestern and southeastern USA and in the Sierra Nevada mountain range of California. Pratt *et al*. (2011) characterized the chemical composition and physical properties of particles emitted from two prescribed burns in Wyoming, in the mountain region of the western USA.

In Finland, prescribed fires have been used since the 1920s but a detailed characterization of aerosols emitted from them has not been done. On 26 June 2009, a prescribed burn of forest slash was conducted about 300–500 m south-southwest of the SMEAR II measurement station (Station for Measuring Ecosystem–Atmosphere Relations; Hari and Kulmala 2005) in Hyytiälä, Finland. Our goals were to study aerosol chemical composition and physical characteristics, concentrations of gaseous compounds, their processes, and modeling atmospheric dispersion of the fire plume (Virkkula *et al*. 2014). Measurements were conducted on the ground using both fixed and mobile instrumentation. Vertical and horizontal dispersion were measured with instruments installed in a Cessna 172 research aircraft. Some results of the airborne measurements were presented in the overview paper (Virkkula *et al*. 2014), and here the data are analyzed in more detail. The focus of the present paper is the analysis of the smoke plume crossings. The goal is to answer the following questions: (1) how do the measured aerosol properties evolve during their transport from the burning area? (2) what are the estimated emission factors of particles and carbon dioxide? and (3) what kind of differences are observed between the aerosols during the flaming phase and the residual smoldering combustion? The coordinates of the most obvious plume crossings are given for possible future use as field data when modeling transport of smoke from the experiment.

Measurements and methods

Instruments

Vertical and horizontal dispersion were measured with instruments installed in a Cessna 172; the setup was described in detail by Schobesberger *et al*. (2013). The sample inlet was similar to the University of Hawai'i shrouded solid diffuser inlet (McNaughton *et al*. 2007). The sample air was transported to the instruments through stainless steel tubing and the air flow was provided by the forward movement of the aircraft together with a venturi tube mounted outside after the instruments. A GPS receiver was used on board to track the airplane's latitude, longitude, and altitude above sea level at a time resolution of one second. Below, the term height is the difference between the altitude of the aircraft and the elevation of the center of the burned area, i.e. 160 m a.s.l.

There were three condensation particle counters (CPCs) for measuring particle number concentrations at three cut-off diameters (3, 6 and 10 nm), i.e. diameters with a 50% detection efficiency. The 3-nm cut-off diameter was with a TSI model 3776 CPC that measures concentrations up to 3×10^5 cm^{-3} with the live-time coincidence correction with a 10% uncertainty and concentrations up to 1×10^6 cm^{-3} with a higher uncertainty. Concentrations between 3×10^5 and 1×10^6 cm^{-3} are underestimated due to coincidence errors, and the CPC should be calibrated against a reference, such as an electrometer. However, this was not done for the unit used in the campaign but for another similar CPC at the University of Helsinki. At the reference number concentrations $N_{ref} = (4.0 \pm 0.3) \times 10^5$ cm^{-3}, $(5.2 \pm 0.2) \times 10^5$ cm^{-3}, $(6.0 \pm 0.3) \times 10^5$ cm^{-3}, $(7.1 \pm 0.2) \times 10^5$ cm^{-3}, $(8.1 \pm 0.3) \times 10^5$ cm^{-3} and $(9.3 \pm 0.3) \times 10^5$ cm^{-3} (mean ± SD), the detection efficiencies, i.e. the ratios of the number concentration measured with the CPC (= N_{3776}) to N_{ref} were 0.98 ± 0.02, 0.95 ± 0.01, 0.91 ± 0.01, 0.86 ± 0.02, 0.80 ± 0.02 and 0.72 ± 0.01, respectively. A correction function $f_{corr} = N_{ref}/N_{3776}$, i.e. the inverse of the detection efficiency was fit to the calibration data and used for correcting data at $N_{3776} > 3 \times 10^5$ cm^{-3}, so that $N_{corrected} = f_{corr} \times N_{original}$, where $N_{original}$ and $N_{corrected}$ refer to the measured and corrected particle number concentration, respectively. The function used for the fitting was a fourth order polynomial.

The other two counters were TSI model 3772 CPCs that measure concentrations up to 10^4 cm^{-3} with the live-time coincidence correction. They were equipped with 1:10 diluters, so the concentrations measured with them has less than 10% uncertainty up to 1×10^5 cm^{-3}. The nominal particle size cutoff diameter of the model 3772 is 10 nm, but the other unit's cutoff diameter was set to 6 nm by changing the temperature difference between the condenser and the saturator. However, the model 3772 CPCs did not work properly during the first flight due to too much butanol filling, so for the first flight the discussion of particle number concentrations is based on the model 3776 CPC only. For the other two flights, data from all three CPCs are discussed. Below the number concentrations of particles measured with the model 3776 CPC and model 3772 CPCs with the cutoff sizes 6 nm and 10 nm are denoted as N3, N6, and N10, respectively. The data of CPCs were saved at 1 Hz frequency.

The particle light scattering coefficient (σ_{sp}) at the wavelength, λ, of 545 nm was measured with a Radiance Research model 903 nephelometer. It was calibrated with CO_2 in the laboratory before the experiment. The peak-to-peak noise of the 2-second data was ~1 Mm^{-1}. The data were corrected for the temperature and pressure and presented at STP conditions (1013 mbar, 0 °C). The particle light absorption coefficient (σ_{ap}) was measured with a Radiance Research 3-λ Particle Soot Absorption Photometer (PSAP) at λ = 467 nm, 530 nm and 660. The data of both the nephelometer and the PSAP were saved at the frequency of 1 Hz. The PSAP firmware was configured to calculate the non-scattering-corrected absorption coefficients by using the factors presented by Ogren (2010). The scattering-corrected value of σ_{ap} was calculated by using the iterative method (Virkkula *et al*. 2005) with the corrected parameter values (Virkkula 2010). The procedure requires scattering coefficients. Since σ_{sp} was available for one wavelength only, σ_{ap} was interpolated logarithmically to λ = 545 nm by using the Ångström exponent of absorption (α_{ap}) that was calculated by fitting the line $\ln[\sigma_{ap}(\lambda)] = -\alpha_{ap}\ln(\lambda) + C$ to the absorption coefficients output directly by the PSAP. The noise of the PSAP 1-second data was ~5 Mm^{-1}. The PSAP filters were changed after the first flight. At the end of the flight the green light (λ = 530 nm) transmittance through the filter had reduced to 0.62. The data were corrected for spot size and flow calibrations.

A LI-COR LI-840 was used for measuring CO_2 concentrations. The data were saved at 1 Hz frequency. The accuracy of the instrument is better than 1.5% and RMS noise < 1 ppm with 1-second signal filtering. The instrument was calibrated at the University of Helsinki before the campaign.

In addition to the airborne measurements, some ground-based measurement data presented in the overview paper (Virkkula *et al*. 2014) are used here. A 3-D sonic anemometer (ATI Sx-Probe) and Vaisala GMP-343 CO_2 sensor were placed within the burn area on the top of a pole at the height of about 12 m. The sonic

anemometer yielded the vertical flow velocity, v_{z0}, that was used here for estimating the emission factors. The CO_2 sensor was used here for estimating the maximum CO_2 concentration in the fire. The aerosol optical measurements at SMEAR II were described in detail by Virkkula *et al*. (2011). In short, the values of σ_{sp} were measured with a TSI 3-λ nephelometer and averaged over 5-min periods. A Magee Scientific 7-λ Aethalometer (AE-31) was used for measuring light absorption, also at a 5-min averaging time. The values of σ_{ap}, single scattering albedo and α_{ap} were calculated from aethalometer and nephelometer data.

Effective scattering cross section diameter

Since there was no instrument measuring the particle size distribution on board the aircraft, the data obtained from the nephelometer and the particle counter were used for getting some measure of the size. For a monodisperse particle size distribution, the light scattering coefficient was calculated from the relation $\sigma_{sp} = NQ_sA_p \equiv NC_s$, where N is the particle number concentration, A_p is the geometric cross section of the particles, Q_s is the particle scattering efficiency, and C_s is the scattering cross section of the particles. C_s is a hypothetical area by which the particle scatters light and, depending on the scattering efficiency Q_s, it may be either larger or smaller than A_p. If it is assumed that the particles are spherical, the diameter of the scattering cross section, D_{Csca}, can be calculated from

$$D_{Csca} = \sqrt{\frac{4}{\pi}C_s} = \sqrt{\frac{4}{\pi}\frac{\sigma_{sp}}{N}}. \quad (1)$$

However, real atmospheric aerosol size distributions are not monodisperse. Therefore, the diameter obtained from Eq. 1 may be called the effective scattering cross section diameter. The value of D_{Csca} may be either larger or smaller than the geometric mean diameter of a size distribution. For a monomodal lognormal size distribution, it is straightforward to show that when the geometric standard deviation remains the same and the geometric diameter increases, then also the value of D_{Csca} increases.

Calculation of the widths of the plume crossings during the flaming-phase flight

During flight 1, there were several smoke plume crossings where the particle number concentrations, scattering and absorption coefficients and carbon dioxide concentrations increased significantly. The CPC was the most sensitive instrument. There were also short particle number concentration peaks with no increased scattering and absorption coefficients and CO_2 concentrations. For the plume crossing analyses, only those crossings were taken in which all the measured quantities had a clear beginning and end, and where the number concentration of particles larger than 3 nm (N3) was above 10^4 cm^{-3}. There were 26 of them. Each plume crossing was analyzed separately. For all the measured parameters, the important value was the excess concentration of species X. The minimum concentration before and after the plume crossing was taken as the background concentration and the excess concentration, ΔX, was the difference between the measured and the background concentration. The width of each plume crossing was determined from the CPC, the PSAP, and the GPS coordinate data as the full width at half maximum (FWHM) of ΔX. The obtained plume crossing widths were used for calculating the area of the plume cross section by assuming it was circular.

Redistribution of scattering coefficient and carbon dioxide concentrations

The CO_2 concentration and scattering coefficients were not used for the determination of the plume crossing widths, since they reached maximum values during each plume crossing always a few seconds later than the CPC and the PSAP, and their peaks were also broader, as is shown in the results. A plausible explanation is that the CPC and PSAP measure essentially without a time lag, with their peak shapes being almost identical, whereas the CO_2 monitor and nephelometer have a finite measurement volume that needs to be filled, making their response times slower. If a plume crossing is quick, cleaner air

starts getting into the measurement volume of these latter two instruments even before the maximum value is reached. It is therefore reasonable to claim that the respective CO_2 concentrations and scattering coefficients were underestimated.

In order to make quantitative estimates of the true values, it was assumed here that (1) the plume shape detected with the faster instruments (CPC and PSAP) was correct, and (2) the time integrals of the peaks were correct with the nephelometer and the CO_2 monitor. Using this information, the CO_2 concentration and the scattering coefficient time series were redistributed to the peak shapes averaged from those of the CPC and the PSAP.

Modeling transport time and the applications

Aerosol processes are time dependent, so for evaluating them it is necessary to have an estimate of the time that passed between the emission of the smoke and each plume crossing by the aircraft. Here, the time elapsed since the smoke was emitted (the time since emission) was estimated with a plume rise model BUOYANT presented by Kukkonen *et al*. (2014). The model addresses the variations of the cross-plume integrated properties of a highly buoyant plume in the presence of a vertically varying atmosphere. The model also includes a treatment for a rising plume interacting with an inversion layer. Kukkonen *et al*. (2014) compared the model predictions with the data of two prescribed wild-land fire experiments. These were the "Smoke, Clouds and Radiation — California" experiment, SCAR-C, in the U.S. in 1994 (Kaufman *et al*. 1996), and the Hyytiälä prescribed burn experiment analyzed here. The results of the comparison show that the model can be used with a fairly good accuracy for evaluating the dispersion from major wild-land fires.

The model follows the plume and yields for each time step since the emission the horizontal distance from and the height above the burn area center, as well as the horizontal and vertical velocities. The modeled time was used for assessing the contribution of coagulation to the decrease of particle number concentration and particle growth. Due to the lacking particle size distribution measurements, only the simple monodisperse coagulation was considered. It is straightforward to show (e.g. Hinds 1999, 2001) that in this case particle number concentration decreases with time, t, according to

$$N(t) = \frac{N_0}{1 + N_0 K t} \quad (2)$$

and that the particle diameter, D_p, increases according to

$$D_p(t) = D_{p0}(1 + DN_0 K t)^{1/3}, \quad (3)$$

where N_0 and D_{p0} are the particle number concentration and particle diameter at the beginning of the process and K is the coagulation coefficient.

Emission factor estimates

Trace gas and aerosol emissions can be expressed as an emission factor (EF = m_X/m_{BM}) which means the mass of emitted species X divided by the mass of burned biomass (m_{BM}). The value of m_{BM} was estimated as in Virkkula *et al*. (2014). The emitted mass of CO_2, number of particles, black carbon and organic carbon were estimated by combining information from the airborne measurements and the vertical velocity (1) measured on ground in the middle of the burning area, and (2) modeled with the BUOYANT. In both methods the mean excess concentration (ΔX_i) of CO_2, BC, particle number and POM in each plume crossing i was multiplied by the plume cross-section area A_i, which was calculated from the crossing diameter by assuming that the cross section is circular.

In the method using the ground-based measured vertical flow velocities, a linear regression was calculated between height and the product $\Delta X_i A_i$. The regression yields the offset $\Delta X_0 A_0$ that is the value of the product at the ground level. Next, the information on the vertical velocity, v_{z0}, measured in the middle of the fire at the altitude of 12 m above ground was used. During fire front crossing the mean ± SD of v_{z0} was 4.5 ± 2.2 m s^{-1} (Virkkula *et al*. 2014), which was the value used in our estimates. The total mass emitted

was estimated by multiplying $\Delta X_0 A_0$ with v_{z0} and interagrating this over the flaming phase time $t_F \approx 2$ h 15 min. If it is assumed that both $\Delta X_0 A_0$ and v_{z0} remain constant during the burning, the emitted mass, m_{TOT}, is

$$m_{TOT} = \int_0^{t_F} \Delta X_0 A_0 v_{z0} dt \approx \Delta X_0 A_0 v_{z0} t_F \quad (4)$$

The method using the BUOYANT is almost similar. The main difference is that the modeled vertical velocities v_{zi} at each height were used for estimating the flux $F_i = \Delta X_i A_i v_{zi}$ through each plume crossing. A linear regression between height and F_i yields the flux at the ground level, F_0, and the emitted mass is calculated from $m_{TOT} = F_0 t_F$.

For calculating the CO_2 emissions, the concentration of CO_2 was converted into mass concentrations. At 20 °C and 1013 mbar, 1 ppm of CO_2 equals 1.83 mg m^{-3}. For calculating the BC emissions, the absorption coefficients were converted into mass concentrations of black carbon (BC) by dividing σ_{ap} by the mass absorption coefficient MAC = 7.7 m^2 g^{-1} at λ = 545 nm. An instrument used widely for BC measurements, the Multi-Angle Absorption Photometer (MAAP), uses MAC = 6.6 m^2 g^{-1} at λ = 637 nm. If it is assumed that particles are pure black carbon it is MAC varies approximately inversely with wavelength (e.g. Bond and Bergstrom 2006). By using the above MAC value and assuming that it is inversely related to wavelength, MAC = (7.7 ± 1.2) m^2 g^{-1} at λ = 545 nm, where the uncertainty is that given by Bond *et al*. (2013). The scattering coefficients were used to estimate particulate organic matter (POM) by dividing σ_{sp} by the mass scattering coefficient (MSC) of (3.1 ± 0.8) m^2 g^{-1} presented by Hand and Malm (2007) for fine mode remote and rural continental POM.

The combined uncertainties of the emission factors were calculated from

$$\delta EF = \sqrt{\sum_i \left(\frac{\partial EF}{\partial x_i} \right)^2 (\delta x_i)^2} \quad (5)$$

where δx_i is the uncertainty of variable x_i. The uncertainties considered were those of the measurements (δN3, $\delta\sigma_{sp}$, $\delta\sigma_{ap}$, δCO_2), the uncertainty of the mass scattering coefficient (δMSC) in the POM estimate, the uncertainty of mass absorption coefficient (δMAC) in the BC estimate, the uncertainty of the mass of burned biomass (δm_{BM}), the uncertainty of vertical velocity (δv_z), the uncertainty δEF_R that is obtained from the standard error in the linear regression of height *vs*. the product $\Delta X_i A_i$ and of height *vs*. the flux F_i. and the uncertainty of the time of the flaming phase δt_F. The uncertainties of the surface areas of the plume crossings and the variability of the emission power are the dominant factors in δEF_R so these were not explicitly written in the formulas. With these assumptions, it is straightforward to show that the uncertainties of the emission factors of N3, POM, BC, and CO_2 can be estimated from

$$\delta EF_{N3} = EF_{N3} \sqrt{\left(\frac{\delta N3}{N3}\right)^2 + \left(\frac{\delta m_{BM}}{m_{BM}}\right)^2 + \left(\frac{\delta v_z}{v_z}\right)^2 + \left(\frac{\delta EF_R}{EF_R}\right)^2 + \left(\frac{\delta t_F}{t_F}\right)^2} \quad (6)$$

$$\delta EF_{POM} = EF_{POM} \sqrt{\left(\frac{\delta \sigma_{sp}}{\sigma_{sp}}\right)^2 + \left(\frac{\delta MSC}{MSC}\right)^2 + \left(\frac{\delta m_{BM}}{m_{BM}}\right)^2 + \left(\frac{\delta v_z}{v_z}\right)^2 + \left(\frac{\delta EF_R}{EF_R}\right)^2 + \left(\frac{\delta t_F}{t_F}\right)^2} \quad (7)$$

$$\delta EF_{BC} = EF_{BC} \sqrt{\left(\frac{\delta \sigma_{ap}}{\sigma_{ap}}\right)^2 + \left(\frac{\delta MAC}{MAC}\right)^2 + \left(\frac{\delta m_{BM}}{m_{BM}}\right)^2 + \left(\frac{\delta v_z}{v_z}\right)^2 + \left(\frac{\delta EF_R}{EF_R}\right)^2 + \left(\frac{\delta t_F}{t_F}\right)^2} \quad (8)$$

$$\delta EF_{CO_2} = EF_{CO_2} \sqrt{\left(\frac{\delta CO_2}{CO_2}\right)^2 + \left(\frac{\delta m_{BM}}{m_{BM}}\right)^2 + \left(\frac{\delta v_z}{v_z}\right)^2 + \left(\frac{\delta EF_R}{EF_R}\right)^2 + \left(\frac{\delta t_F}{t_F}\right)^2} \quad (9)$$

The absorption coefficient and thus the estimated BC emissions have also an additional source of uncertainty. Cappa *et al*. (2008) and Lack *et al*. (2008) analyzed the bias in the light absorption coefficient measured with a PSAP

compared with a non-filter-based reference method, a photoacoustic spectrometer ($\sigma_{ap,ref}$). In both of these studies it was found that at high organic aerosol loadings the PSAP overestimated absorption and that this overestimation can be more than a factor of two. In the middle of the smoke plume this bias can be even higher than that. Lack *et al*. (2008) also presented a parameterization for the bias

$$\frac{\sigma_{ap,PSAP}}{\sigma_{ap,ref}} = 0.032\frac{m_{POM}}{m_{BC}} + 1.3, \qquad (10)$$

If the concentrations are estimated from $m_{POM} = \sigma_{sp}$/MSC and $m_{BC} = \sigma_{ap,ref}$/MAC by using the above-mentioned values, MSC = 3.1 m^2 g^{-1} and MAC = 7.7 m^2 g^{-1}, Eq. 10 can be reorganized and simplified to

$$\sigma_{ap,ref} = 0.77\sigma_{ap,PSAP} - 0.061\sigma_{sp} \qquad (11)$$

where $\sigma_{ap,PSAP}$ is the absorption coefficient calculated by using the algorithm presented by Virkkula (2010). Below the absorption coefficients, single-scattering albedos, and BC emission factor estimates are calculated both with and without applying Eq. 11.

Results and discussion

Overview of the experiment

Approximately a 0.8 ha was cut clear in February 2009. The coordinates of the center of the clear-cut area were 61.84378°N, 24.29345°E, and the elevation 160 m a.s.l. After the clear-cut, remaining slash including some tree trunks, all treetops and branches were left on the ground to be burned. The measurement setup was ready at the beginning of May 2009, waiting for proper conditions for the experiment. The conditions were right on the morning of 26 June: wind was blowing at less than 5 m s^{-1} from the right direction (175°–215°) to blow smoke to the ground-based instrumentation at SMEAR II, the sky was clear, and soil was dry. Relative humidity and temperature at 4.2 m above ground was 56% and 19 °C, respectively. The fire was ignited at 07:45 East European Time (EET = UTC + 2h). All times presented below are in EET. The flaming or active burning was over at 10:00 EET, i.e. in about 135 minutes. After the main burning, the ground was smoldering and there was only a little visible smoke at 13:00 EET. The end times of the flaming and smoldering periods are not well defined: there were flames in some parts of the area while most of it was already smouldering, and smouldering biomass does not always emit visible smoke. To be accurate, the periods should be called flaming-dominated phase and smoldering-dominated phase. However, for simplicity and to be consistent with the overview paper (Virkkula *et al*. 2014), only the terms flaming phase and smouldering phase are used here.

During the flaming phase, most of the smoke ascended almost vertically, as shown in the aerial photographs in Virkkula *et al*. (2014), indicating that wind speed was not high and no strong temperature inversion was present to inhibit the rising smoke. At the ignition time, wind speed was < 2 m s^{-1} at all altitudes of the SMEAR II 73-m mast, but it increased to 2–4 m s^{-1} during the morning.

After the burning, the amount of burned organic material was estimated to be 46 800 ± 10 900 kg (for details, *see* Virkkula *et al*. 2014). In short, it was calculated as a sum of burned tree biomass, surface vegetation and organic soil layer. This value was used in the present paper for the estimates of emission factors of particles and carbon dioxide.

Flight routes and data

Three research flights were conducted during the day: flight 1 from 07:43 to 10:16 EET, flight 2 from 11:03 to 13:39 EET and flight 3 from 15:48 to 17:56 EET (Fig. 1). The first flight took place during the flaming phase, the second during the smoldering phase and the last one when no smoke was visible on the ground. The horizontal distances from the burning area center varied from about 10 m to 50 km because the flights took off and landed at the Tampere Pirkkala airport, about 50 km SW from the burning site.

It was planned that during each flight, the smoke plume would be flown through at several altitudes. This was easy during the first flight, because the smoke was visible and the

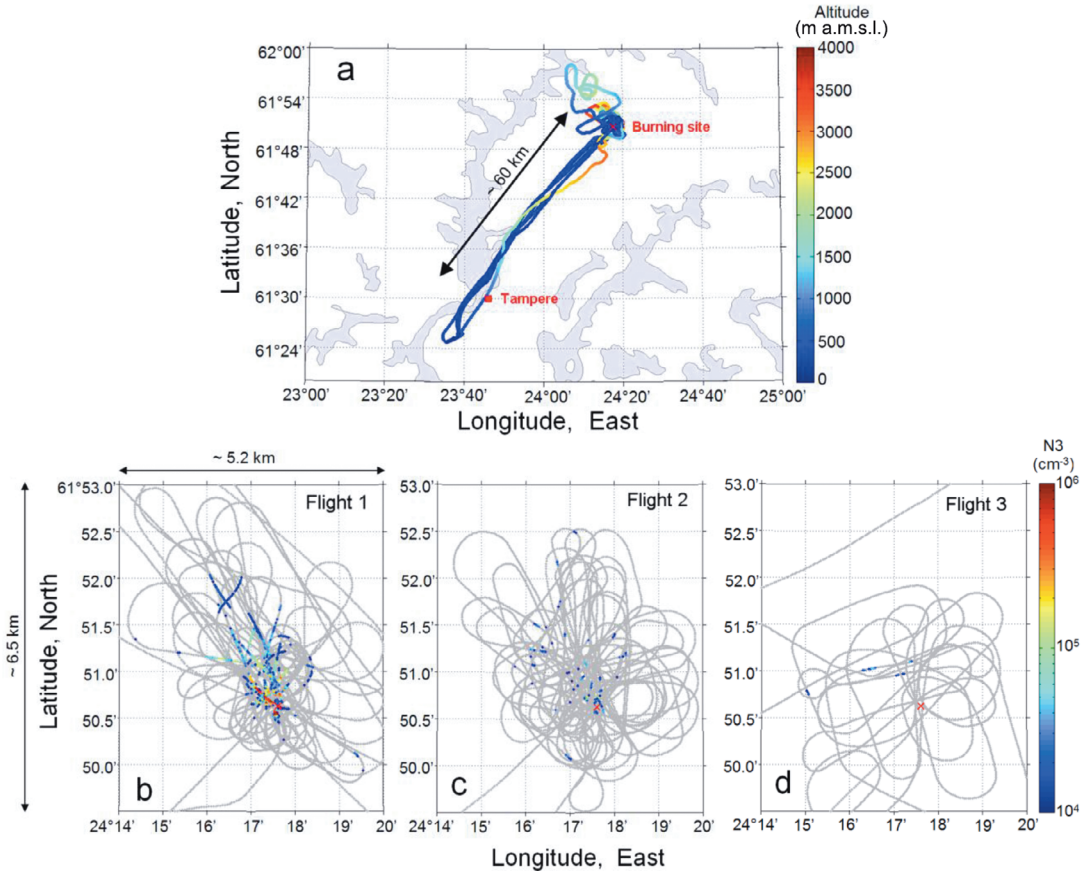

Fig. 1. Routes of the research flights during the experiment: (**a**) the full flight routes from Tampere to Hyytiälä and surroundings with color-coded altitude, and (**b–d**) routes of the three flights in the vicinity of Hyytiälä with number concentration of particles larger than 3 nm (N3) coded with colors (grey line: N3 < 10^4 cm^{-3}, colored line: N3 > 10^4 cm^{-3}).

plume was detected by all methods: as particle number concentrations rose up to ~10^5–10^6 cm^{-3}, elevated scattering and absorption coefficients reached values higher than 1000 Mm^{-1}, and CO_2 concentrations exceeded the then background concentrations by ~100–300 ppm. Below, the data collected during flight 1 are analyzed first in detail, and the number concentrations measured during flights 2 and 3 in a subsequent section. During the smoldering-phase flights, the concentrations were lower and the plume was not visible, even though the particle number concentrations exceeded 10^4 cm^{-3} (Fig. 2). The CO_2 monitor did not detect any peaks above the baseline then, while the nephelometer and the PSAP only a few. There were only very small excess absorption coefficient values during flight 2. The PSAP was removed from the aircraft after flight 2, so there are no absorption data from flight 3.

During flight 1, high particle number concentrations were measured up to a height of about 1500 m above ground level (a.g.l.) even though a single 3-second concentration peak was recorded at 2400 m a.g.l. (Fig. 3). In this peak, only the values of N3 were high, while the scattering and absorption coefficients and the CO_2 concentrations did not vary at all. At the lowest flight levels, N3 was occasionally higher than 3 × 10^5 cm^{-3} but during the other two flights it was always less than this value (Fig. 3). Horizontally, high concentrations were recorded at about 3–4 km from the centre of the burn area (Fig. 3).

Note that for flight 1, the CO_2 and the σ_{sp} data were plotted both with a black and red line

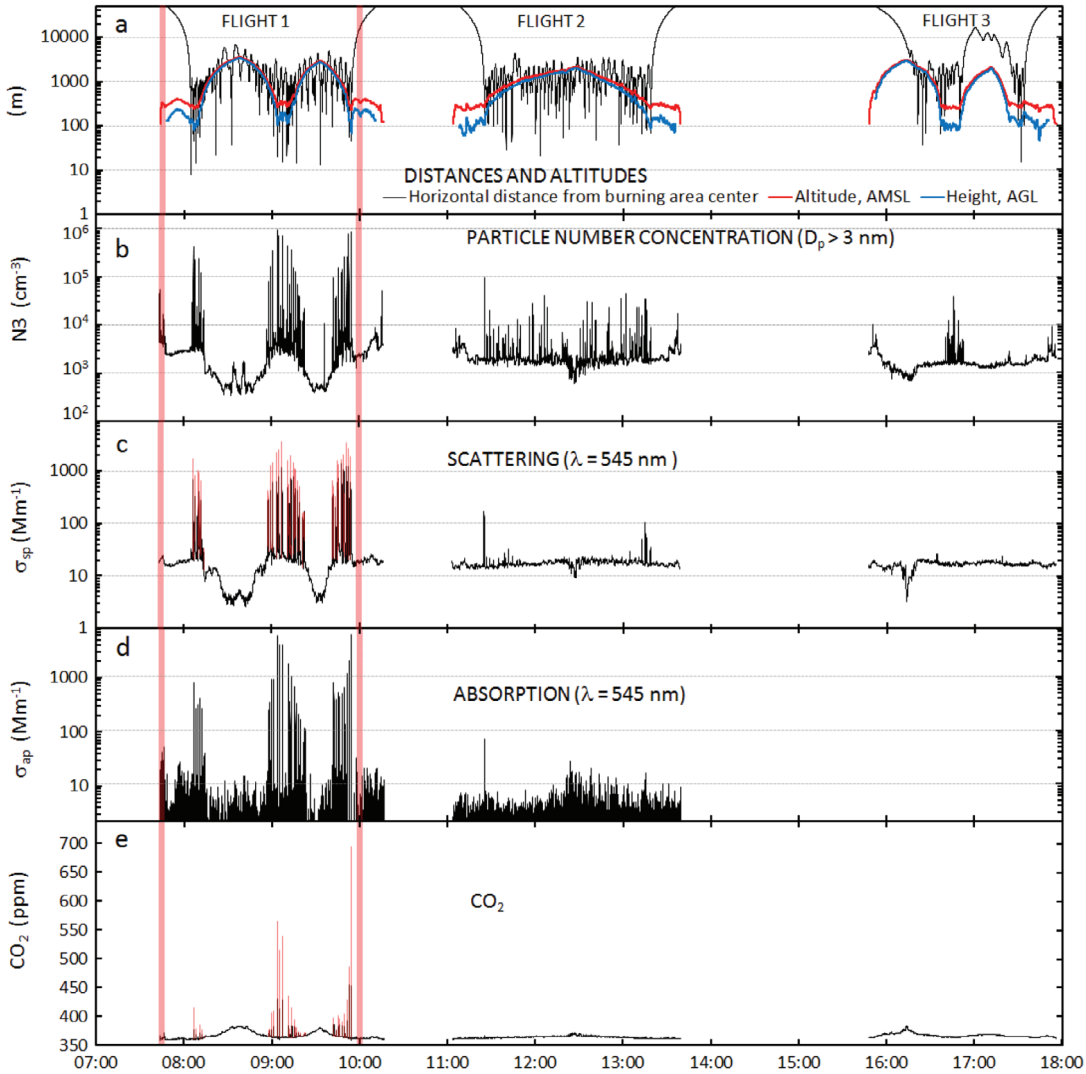

Fig. 2. Airborne data measured during the three flights of the campaign. (**a**) The horizontal distance from the center of the burning area, altitude above mean sea level (AMSL) and height above ground level (AGL), (**b**) number concentration of particles larger than 3 nm, (**c**) scattering coefficient, (**d**) absorption coefficient, and (**e**) carbon dioxide concentrations. The scattering coefficient and the carbon dioxide concentrations are plotted both with a black and a red line. The black lines are the raw data and the red lines the data that were corrected for the slow response time of the instruments. See details in the text. The vertical red lines denote the start and end of the flaming phase of the experiment.

(Fig. 2). The red lines show those values of the CO_2 concentrations and scattering coefficient that were redistributed to the peak shapes averaged from those of the CPC and the PSAP, as explained above. An example of this is shown for six plume crossings in Fig. 4. This leads to the higher concentrations shown in the redistributed data in Figs. 2 and 4.

Smoke plume widths during the flaming-phase flight

The widths of the plume crossings were estimated from the particle number concentrations as described in the measurements and methods section. An example is given on the plume crossing at 09:04:03–09:04:08. At t = 0, 1, 2, 3, 4 and

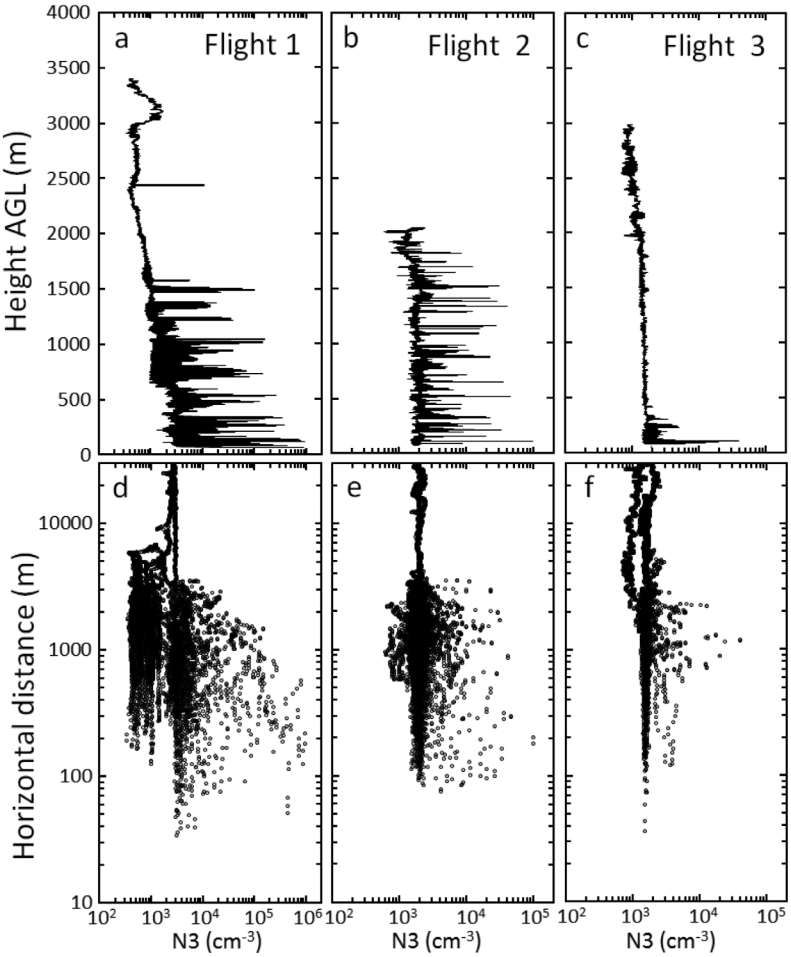

Fig. 3. Number concentrations particles larger than 3 nm during the three flights as a function of (**a–c**) height above ground, and (**d–f**) horizontal distance from the centre of the burn area.

5 s the ΔN3 concentrations were 5.2×10^3, 8.2×10^4, 9.4×10^5, 9.4×10^5, 2.1×10^5, and 9.7×10^3 cm^{-3}, respectively, which is 0.5 %, 8.7 %, 100%, 100%, 22.3%, and 1.0 % of the maximum. The half maximum value was reached at the rising edge somewhere between $t = 1$ s and $t = 2$ s, and at the decreasing edge somewhere between $t = 3$ s and $t = 4$ s. The concentration was higher than half of the maximum value for at least 2 s but less than 3 s. The greater of these times was used, and the mean number concentration in this plume crossing was calculated from the three largest values as $(9.4 \times 10^5 + 9.4 \times 10^5 + 2.1 \times 10^5)$ $cm^{-3}/3 \approx 7.0 \times 10^5$ cm^{-3}. The plane was then flying at a speed of about 139 km h^{-1} (38.6 m s^{-1}), so in 3 s it flew 116 m, which is given as the peak width. If it is assumed that the uncertainty at both the rising and the decreasing edges of the plume crossing is one second, the uncertainty in distance is about 80 m.

The plume crossing data present the locations of 26 smoke-plume crossings during the flaming phase and the mean and maximum excess concentrations observed in them (Table 1). The scattering coefficients and CO_2 concentrations presented in Table 1 were calculated from the redistributed data as explained above. Table 1 can be used for reproducing most of the results presented below. Note, however, that the particle number concentrations presented in Table 1 are those given by the CPC. When calculating the emission factors, the values of N3 larger than 3×10^5 cm^{-3} were multiplied by the calibration correction function f_{corr}.

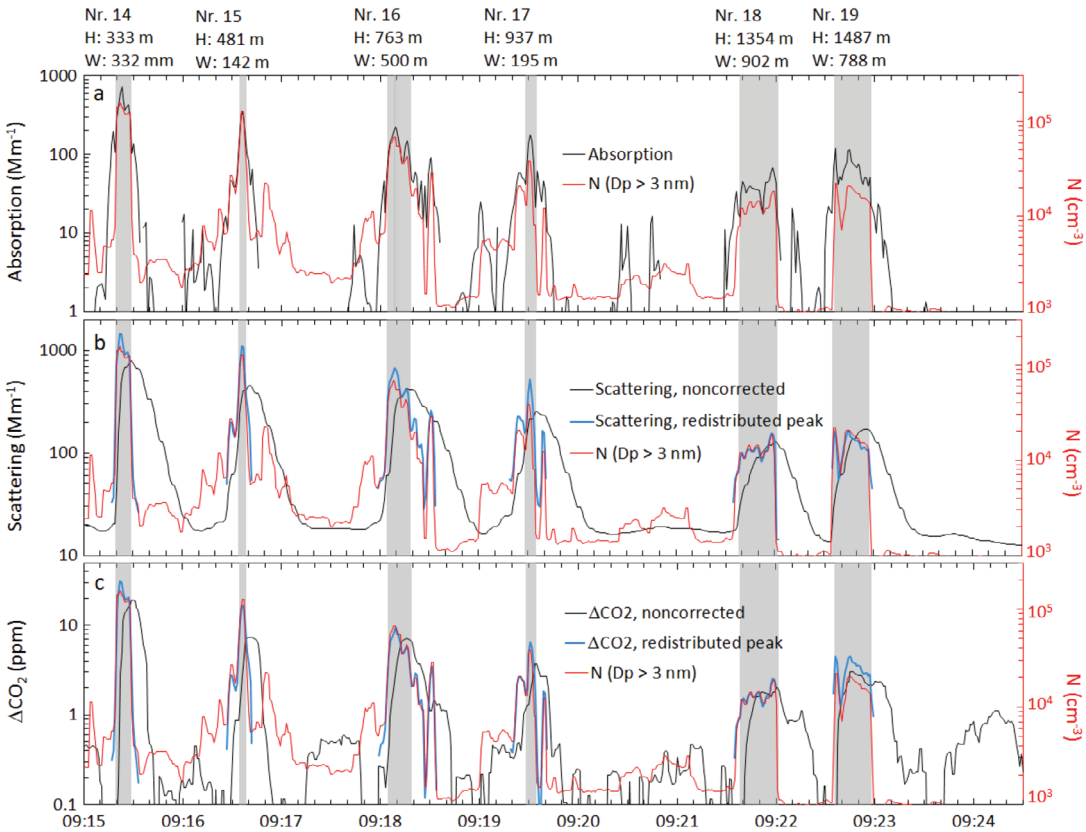

Fig. 4. Airborne data measured during the first flight at 09:15:00–09:24:30 and an example of the redistribution of scattering and carbon dioxide for smoke plume crossing numbers 14–19. The particle number concentration is presented in all panels (*y*-axis on the right). In addition, in **a** the absorption coefficient time series, the serial numbers of the smoke plume crossings, the height above ground level (*H*), the width of the peak (*W*) as full width at half maximum particle number concentration, in **b** the original and the redistributed scattering coefficients, in **c** the original and the redistributed carbon dioxide concentrations. The shading shows the width of the peaks as full width at half maximum.

Evolution of the smoke plume as a function of distance from the fire

The concentrations and aerosol properties are first analyzed as a function of the real distance from the burning area, then as a function of estimated time of transport since the emission. The former approach is more accurate since the position was measured with a GPS and an altimeter whereas the transport time was modeled. For describing the decrease of the concentrations as a function of distance, two forms of equations were fitted to the data: a power law Ax^b and an exponential function Ae^{bx} where x is the distance from the center of the burn area and A and b are parameters to be fitted. For ΔCO_2, the best fit was obtained with the power law as $\Delta CO_2 = 2.8 \times 10^4 x^{-1.06}$ ppm, where x is in meters. For the 12-m altitude, this formula yields the concentration of 2440 ppm, which is in a very good agreement with the measurements from the 12-m mast where the peak concentrations varied from about 2000 to 3000 ppm (Fig. 5a). At distances greater than about 400 m from the burn area, the exponential function fitted the data well. The power fit to the non-redistributed CO_2 concentrations $CO_2 = 918x^{-0.65}$ ppm predicted that at 12 m, the concentration would be 182 ppm, which is an order of magnitude lower than the measurements from the 12-m mast. This indirectly supports the redistributing of concentration data in the plume crossings as described above. It has to be

Table 1. Locations of 26 smoke plume crossings during the flaming phase and concentrations observed in them. LAT and LONG: latitude and longitude in degrees and decimals of degrees; HGHT: height above ground level; Dist: horizontal distance from the burn area centre; *W*: full width at half maximum; ΔN3: mean and maximum excess number concentrations of particles larger than 3 nm; $\Delta\sigma_{sp}$: excess scattering coefficients at λ = 545 nm; $\Delta\sigma_{ap}$: excess absorption coefficients at λ = 545 nm; ΔCO_2: excess carbon dioxide concentrations. Both $\Delta\sigma_{sp}$ and ΔCO_2 are the values redistributed according to the method described in 'Material and methods'.

No.	Plume crossing details										ΔN3		$\Delta\sigma_{sp}$		$\Delta\sigma_{ap}$		ΔCO_2	
	TIME (hh:mm:ss)	LAT (°)	LONG (°)	HGHT (m)	Dist (m)	*W* (m)	t_x (s)	t_z (s)	t_{3D} (s	v_z (m s^{-1})	mean (cm^{-3})	max (cm^{-3})	mean (Mm^{-1})	max (Mm^{-1})	mean (Mm^{-1})	max (Mm^{-1})	mean (ppm)	max (ppm)
1	08:06:56	61.8448	24.2892	84	269	114	63	10	44	5.9	339110	422110	1018	1745	379	659	43	54
2	08:08:04	61.8461	24.2923	97	303	183	70	13	51	5.5	121130	219910	479	801	139	220	14	18
3	08:10:43	61.8462	24.2902	212	372	187	84	40	70	3.5	179500	232060	596	1011	190	320	20	25
4	08:12:08	61.8444	24.2863	303	366	221	83	70	78	2.8	80093	120160	362	648	103	219	9.1	15
5	08:58:15	61.8514	24.2928	706	721	432	150	260	171	1.8	60630	76910	262	401	183	296	10	14
6	08:59:47	61.8455	24.2886	533	336	123	77	168	105	2.0	155900	155900	890	1243	483	791	37	43
7	09:01:07	61.8448	24.2899	339	182	157	45	82	62	2.6	255950	339950	905	1454	458	764	37	46
8*	09:04:05	61.8447	24.2906	120	219	116	53	17	39	4.8	695613	939280	1701	2254	3066	5491	173	202
9	09:05:15	61.8427	24.2922	142	160	149	41	22	33	4.4	541410	704410	1606	2483	2138	3835	119	152
10	09:07:27	61.8446	24.2909	141	179	151	45	22	35	4.4	599690	722190	2446	3641	2012	3751	138	177
11	09:11:21	61.8441	24.2940	122	63	110	20	18	19	4.8	437590	437590	876	1538	771	1729	58	72
12	09:12:29	61.8470	24.2962	168	385	155	87	28	68	4.0	39585	66460	319	533	164	329	13	16
13	09:13:45	61.8459	24.2941	267	223	133	54	57	56	3.0	271310	369060	1199	1961	584	901	41	52
14	09:15:22	61.8486	24.2941	333	604	332	129	80	115	2.7	131081	153970	854	1447	318	593	22	31
15	09:16:36	61.8489	24.2912	481	577	142	124	143	126	2.1	96555	122030	688	1091	179	284	13	17
16	09:18:08	61.8537	24.2893	763	1231	500	241	293	248	1.7	48924	67170	452	653	115	179	6.6	9.5
17	09:19:30	61.8567	24.2862	937	1553	195	297	402	311	1.5	20503	36880	304	491	83	142	4.0	6.5
18	09:21:58	61.8660	24.2792	1354	2394	902	442	702	469	1.3	11683	17487	90	141	32	56	1.7	2.5
19	09:22:36	61.8672	24.2678	1487	2555	788	470	811	503	1.2	15470	21181	107	151	59	106	3.2	4.5
20	09:42:20	61.8552	24.2829	1492	1343	364	261	815	344	1.2	75758	97120	495	641	589	785	25	32
21	09:44:12	61.8533	24.2901	1230	1203	397	236	607	295	1.3	31766	37150	217	303	235	380	8.2	11
22	09:45:36	61.8509	24.2875	1045	863	224	176	474	232	1.5	125630	154690	1150	1532	341	465	27	36
23	09:48:17	61.8494	24.2902	733	831	639	170	275	189	1.7	93324	140980	1140	1658	246	422	18	27
24	09:49:41	61.8481	24.2839	538	754	224	156	170	157	2.0	212920	256140	1406	2056	393	571	35	41
25	09:51:41	61.8448	24.2891	266	304	117	70	57	57	3.0	244257	260590	2220	3474	634	1054	55	66
26*	09:54:20	61.8427	24.2930	68	159	112	41	8	8	6.3	616720	870720	1483	1881	5200	6893	262	332

* The concentrations and uncertainties in plume crossings 8 and 26 were very high, hence they were treated as outliers in emission factor estimations.

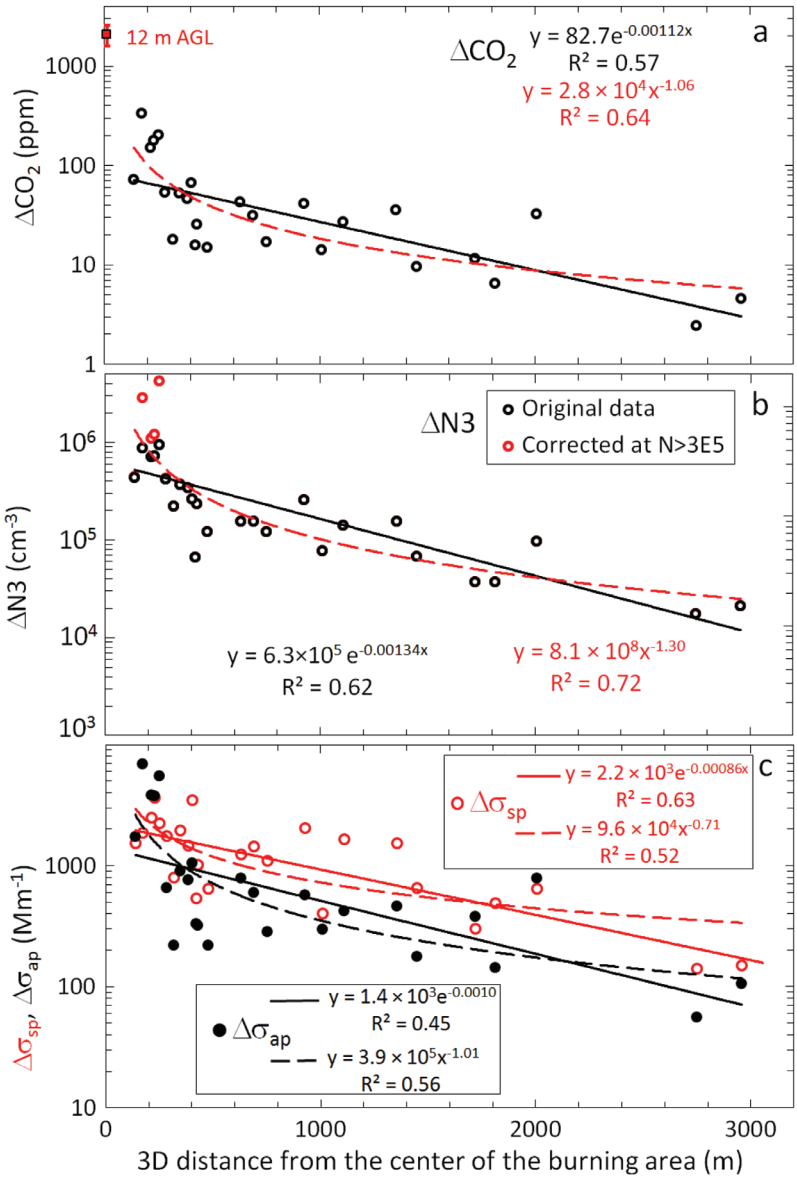

Fig. 5. Decrease in (**a**) maximum excess CO_2 concentration (ΔCO_2), (**b**) maximum excess particle number concentration ($\Delta N3$), and (**c**) maximum excess scattering ($\Delta\sigma_{sp}$) and absorption ($\Delta\sigma_{ap}$) coefficients as a function of 3-dimensional distance from the center of the burning area during flight 1. The solid lines are exponential fits and the dashed lines power function fits to the data. The ΔCO_2 at 12 m AGL denotes the peak concentrations in the 12-m pole within the burning area. The aircraft data points are the maxima in each plume crossing. In **b** the $\Delta N3$ data are the original plume crossing maxima and those corrected according to the calibration of a similar CPC. In **b** the lines were fit to the calibration-corrected data.

noted, however, that the above comparison of the extrapolated concentration with that measured from the 12-m mast intrinsically assumes that the fire power is constant. This of course is not true and explains some of the scatter of the data.

The two highest measured peak excess particle number concentrations, $\Delta N3 = 0.94 \times 10^6$ cm^{-3} and 0.87×10^6 cm^{-3} (Table 1), were higher than in the calibrations mentioned. The respective extrapolated correction functions were $f_{corr} \approx 3.6 \pm 0.8$ and 2.7 ± 0.5, so the estimated peak values of $\Delta N3$ were about $(3.3 \pm 0.8) \times 10^6$ cm^{-3} and $(2.4 \pm 0.4) \times 10^6$ cm^{-3}, respectively. The maximum values of $\Delta N3$ decreased almost exponentially as a function of the distance from the center of the burn area, even though close to the source the power law obviously described this decrease better (Fig. 5b). After the multiplication by f_{corr}, the two highest excess particle number concentrations were in agreement with the ground-based peak concentrations of 2.5×10^6 cm^{-3} measured from the Sniffer van at a dis-

tance of around 180 m from the burn area during the smoldering phase when the smoke did not rise any more (Virkkula *et al*. 2014).

Of all the measured variables, ΔN3 decreased the fastest and scattering coefficient the slowest. This can be described quantitatively by the *e*-folding distances, i.e, the distance over which the quantity decreases by a factor of *e* (2.718). The *e*-folding distances (= 1/*k*) calculated from $C = C_0 e^{-kx}$ where the *k* values presented in the exponential functions in Fig. 5 were 750 ± 120 m, 890 ± 160 m, 990 ± 240 m, and 1160 ± 190 m for the maxima of ΔN3, ΔCO_2, $\Delta\sigma_{ap}$ and $\Delta\sigma_{sp}$, respectively. The error estimates are the standard errors of the values of *k* obtained from the fittings of the exponential functions. The particle number concentration decreased faster than the other quantities, while the scattering coefficient decreased at the lowest rate. This can be explained by the fact that the number of particles is decreasing not only by dilution but also by coagulation in the plume, whereas both CO_2 and absorbing aerosol (black carbon concentration) decrease only by dilution. The processes affecting the scattering coefficient are both dilution and growth of particles by condensation.

The single-scattering albedo, ω_o [= $\sigma_{sp}/(\sigma_{sp} + \sigma_{ap})$], is a measure of the darkness of aerosols: for purely scattering aerosols $\omega_o = 1$. For freshly-generated pure BC, ω_o has been measured to be 0.2 ± 0.1 (e.g., Bond and Bergstrom 2006, Mikhailov *et al*. 2006, Cross *et al*. 2010, Bond *et al*. 2013). In the plume crossings, ω_o apparently increased during the transport from close-to-pure-BC values of about 0.4 ± 0.2 in the crossings closest to the source to about 0.8 ± 0.1 at the distance of about 400 m, which is consistent with that calculated from the ground-based data at SMEAR II during the flaming-phase plumes (Fig. 6a). It is not very credible that condensational growth during such a short distance would be so strong that it would explain such a rapid growth of ω_o, especially considering that the growth of ω_o essentially finished after 400 m. Another probable explanation for the fast increase of ω_o is that the smoke plume crossings at the lowest levels were so fast that the nephelometer still underestimated scattering even after the redistribution procedure. However, there were two plume crossings with $\omega_o \approx 0.5$ as far as ~1–2 km from the center of the burning area even after the redistribution procedure and even though the plume crossing was wide enough (~360–400 m), so the values of σ_{sp} were probably not significantly underestimated. This suggests that the optical properties, such as the darkness of the particles emitted from the fire, actually varied with time even at the source. The single-scattering albedos were also calculated by first calculating σ_{ap} from Eq. 11 to estimate the bias by condensing organics shown by Cappa *et al*. (2008) and Lack *et al*. (2008) in affecting filter-based absorption measurements. The values of ω_o were higher than those without using Eq. 11, yet the apparent increase of ω_o with increasing distance remained (Fig. 6a). To quantify the difference when taking into account the crossings at distances > 400 m and excluding the above-mentioned two points, the mean and range (minimum–maximum) of ω_o was 0.82 (0.68–0.91) and 0.74 (0.59–0.82) with and without using Eq. 11, respectively.

The wavelength dependency of absorption is usually presented in the form of the Ångström exponent of absorption (α_{ap}) that gives information on the absorbing material. For pure black carbon (BC) particles, absorption is approximately inversely proportional to the wavelength, in other words $\alpha_{ap} = 1$ (e.g. Van de Hulst 1957, Schnaiter *et al*. 2003), whereas for the aerosol containing organic material α_{ap} is higher (e.g., Kirchstetter *et al*. 2004, Schnaiter *et al*. 2006, Lewis *et al*. 2008). The mean (± SD) value of α_{ap} calculated from the mean non-scattering-corrected absorption coefficients in each plume crossing was 1.70 (± 0.24; Fig. 6b). This value is in line with other observations. For instance, Kirchstetter and Thatcher (2012) showed the spectral absorption of wood smoke filter samples, also without scattering corrections, and obtained the mean value of α_{ap} of 1.9. There were three plume crossings, where α_{ap} was ~1.2, i.e. clearly lower than the mean and closer to the pure BC values. Interestingly, two of them were in the same plume crossings in which $\omega_o \approx 0.5$. This suggests that the low values of ω_o in some plume crossings were not necessarily artifacts but may be due to real variations in particle properties emitted by the fire. The scatter plot of α_{ap} *vs*. ω_o (Fig. 7) supports this interpretation: the two

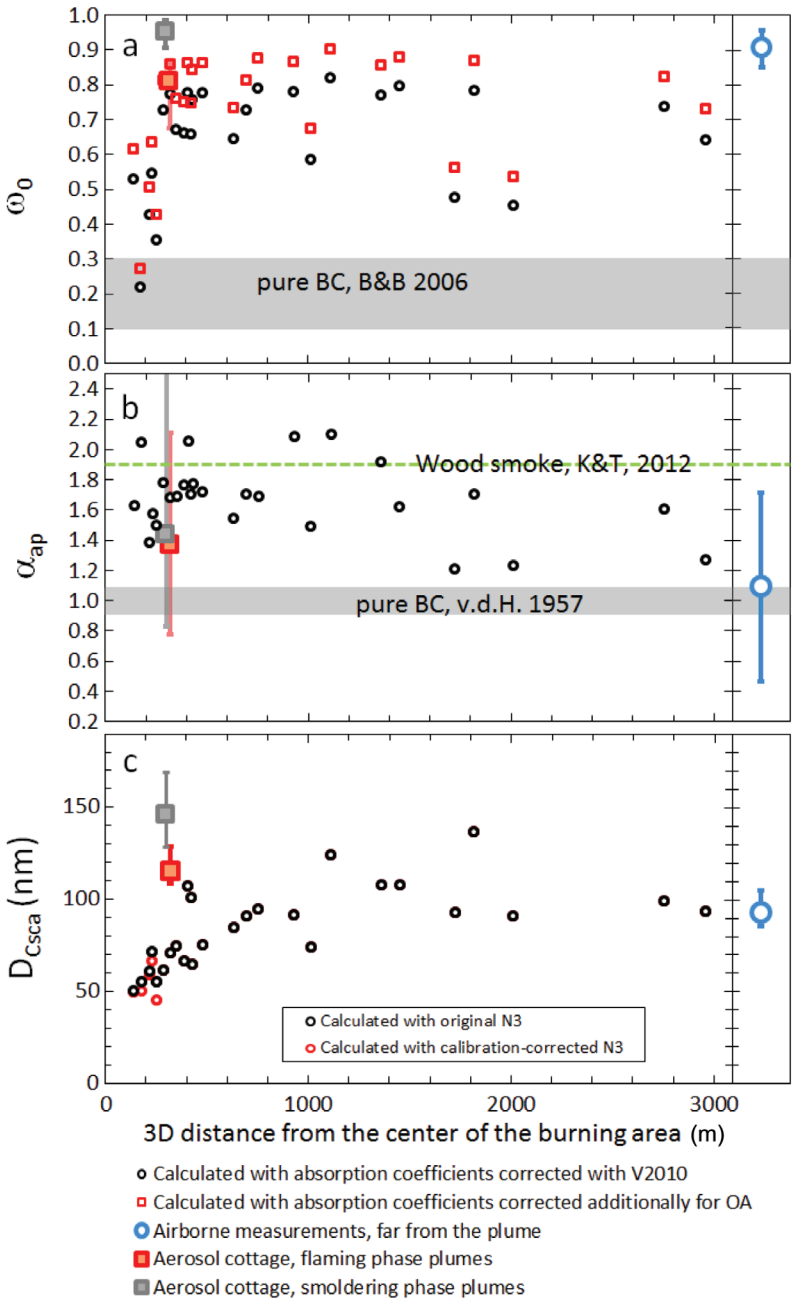

Fig. 6. Intensive aerosol properties in the smoke plume crossings during the flaming-phase flights: (**a**) single-scattering albedo at λ = 545 nm, (**b**) Ångström exponent of absorption in the wavelength range 467–660 nm, (**c**) effective scattering cross section diameter D_{Csca}. The values were calculated from the mean values in each plume crossing. The large squares show respective values calculated from the ground-based measurements at the SMEAR II station. The blue circles show the respective values calculated from airborne measurements far from the smoke plume.

quantities were clearly related to each other, the only obvious outlier being the crossing number 26. The mean value of α_{ap} far from the smoke plume was 1.1 ± 0.6, yet this value is highly uncertain because it was calculated from the 1-s values nearly the detection limit of the PSAP.

Figure 6c shows the effective scattering cross section diameters (D_{Csca}) calculated from Eq. 1 by using the plume-crossing mean scattering coefficients and particle number concentrations (N3) both with and without the calibration correction function, f_{corr}. The correction increased the value of N3 which, according to Eq. 1, led to lower values of D_{Csca}. In the plume crossings with the highest number concentrations, the scattering coefficients were probably underestimated

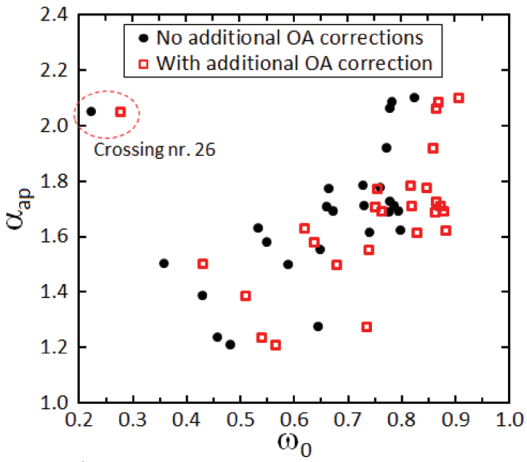

Fig. 7. Ångström exponent of absorption (α_{ap}) *vs.* single-scattering albedo (ω_o) calculated from the mean concentrations in each smoke plume crossing. The black circles: ω_o calculated with σ_{ap} without additional organic aerosol bias correction, red squares: ω_o calculated with σ_{ap} calculated with organic aerosol bias correction (Eq. 11).

even after the redistributions, so also these diameters were probably underestimated. However, the main observation was that D_{Csca} obviously increased during the first 1000 m of transport from ~50 nm to ~100 ± 20 nm. The latter value is in agreement with the ground-based measurements. The scattering coefficients and number concentrations measured from the aerosol cottage of SMEAR II were used to calculate D_{Csca} with the same equation. The mean value of D_{Csca} was 117 ± 8 nm in a smoke plume observed at the cottage during the flaming phase. In the smoke observed during the smoldering phase, the value of D_{Csca} was larger (148 ± 15 nm).

Temporal evolution of the smoke plume

The time since emission was estimated with the plume rise model BUOYANT that calculates horizontal and vertical transport of the smoke plume. The model does not yield an unambiguous time passed, since the emission to the time the plane crossed the plume. For any time passed since the emission of a smoke parcel, the model yields its height above the burn area center (continuous line in Fig. 8a). The heights of the actual plume crossings were measured. With these data the vertical time of transport (t_z) since the emission was estimated for each plume crossing. The model also yields the horizontal location of a smoke parcel at any time since the emission. The horizontal transport time (t_x) was calculated for each actual horizontal distance of a plume crossing measured with the GPS (Fig. 8b). And finally, since the model yields both horizontal distance and height, the distance of the smoke plume at any given time can be calculated. The transport time since emission (t_{3D}) was calculated for each plume crossing with this information (Fig. 8c and Table 1). If the model predicted perfectly the plume transport, the measured locations of the plume crossings would yield $t_z = t_x = t_{3D}$. However, it is obvious from Table 1 that the three times were not equal. At heights below about 300 m a.g.l., the modeled values of t_z were smaller than those of t_x while at higher levels they were greater. There was no independent information of which time would be the correct one, so all three transport time estimates are used below.

The transport times were used here for evaluating whether the observed decrease in the particle number concentrations and increase in D_{Csca} could be due to coagulation. These calculations were made according to Eqs. 2 and 3 by using the coagulation coefficient of particles with the diameter of 50 nm, $K = 9.9 \times 10^{-16}$ m^3 s^{-1} (e.g. Hinds 1999, 2001). For larger particles K is smaller, which leads to slower rate of decrease in the particle number concentration and slower rate of growth in the particle size, so the modeled decreases of N and increases of D_p can be considered as upper estimates. The modeling was done by using three different initial number concentrations: 1×10^6 cm^{-3}, 2×10^6 cm^{-3}, and 5×10^6 cm^{-3}, and one initial diameter, $D_{p0} = 50$ nm.

The measured number concentrations decreased considerably faster than they would do due only to coagulation (Fig. 9a), which suggests that dilution was the main mechanism leading to the observed decrease. The particle growth mechanism was evaluated in a similar way. The recorded increase of D_{Csca} was faster than if coagulation were the only growth mechanism (Fig. 9b). For instance, over the time interval from 300 s to 360 s the curve fitted to the data [$D_{Csca}(t_{3D}) = 27 t_{3D}^{0.24}$, Fig. 9b] yielded a particle growth rate of 4.7 nm min^{-1}. Coagulation

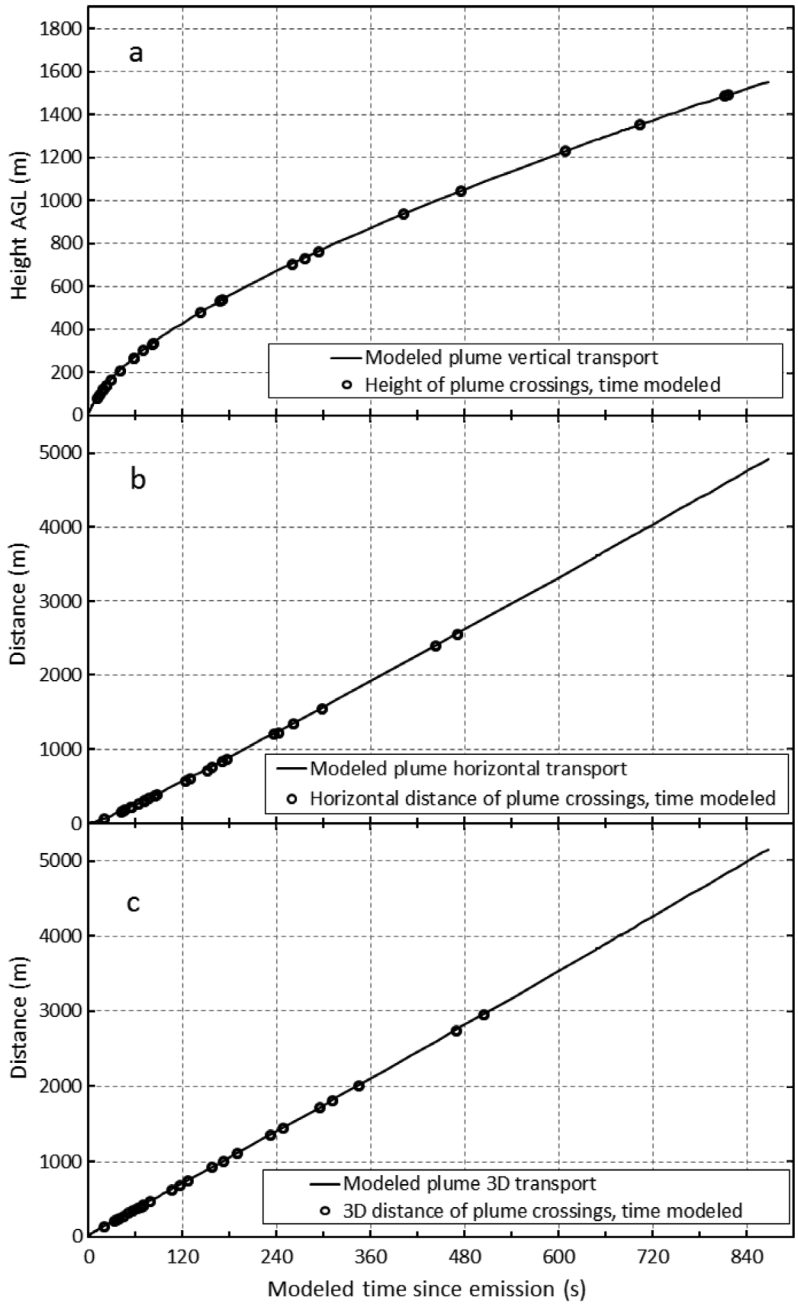

Fig. 8. Time passed between the emission of smoke and arrival at any (**a**) height above the burn area, (**b**) horizontal distance from the burn area center, and (**c**) real distance from the burn area center.

would yield a growth rate of 2.6 nm min^{-1} over the same time interval with the assumptions that the coagulation coefficient was constant and initial particle concentration was 5×10^6 cm^{-3}. The value of D_{Csca} increased faster than could be explained by coagulation, which suggests that condensation played an important role in the particle growth even at the early stages of the smoke plume. However, the uncertainty in D_{Csca} was the highest in the narrowest plume crossings, scattering being probably underestimated, which might lead to an underestimation of D_{Csca} in the beginning and overestimation of its increase rate. No quantitative estimates of the contributions of

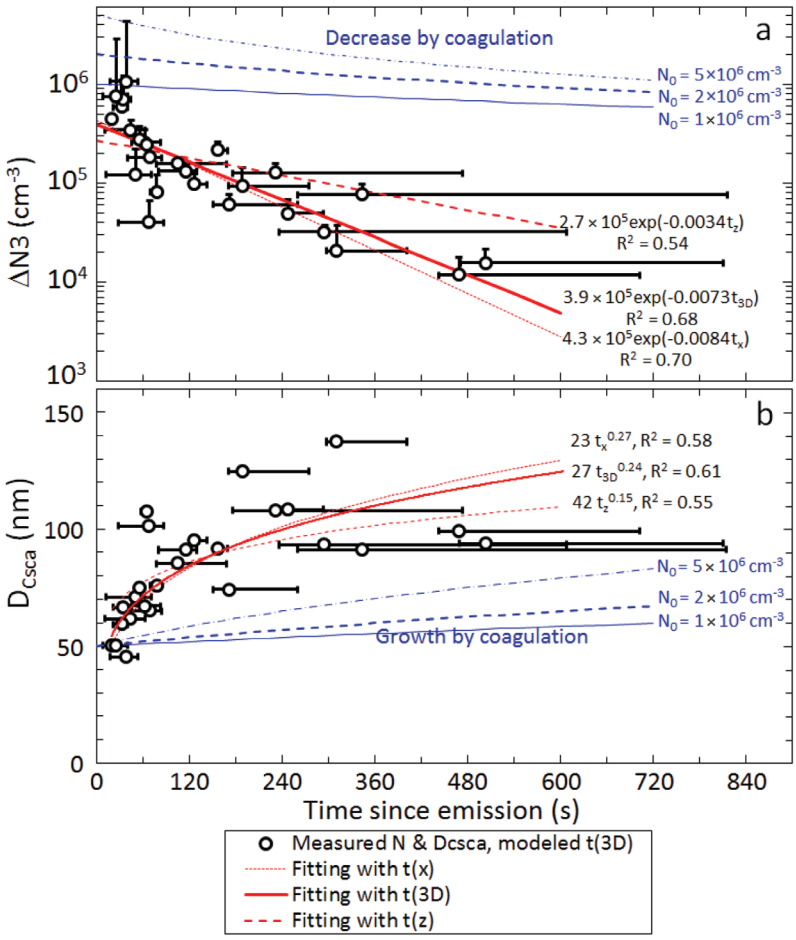

Fig. 9. Temporal evolution of (**a**) excess number concentration (ΔN3) and (**b**) effective scattering cross section diameter (D_{Csca}). The *y*-axis value of the circle is the mean ΔN3 and D_{Csca} in each smoke plume crossing, the *x*-axis value is the modeled transport time since emission (t_{3D}). The vertical error bars of ΔN3 show the maxima in each crossing, the horizontal error bars show the minimum and maximum modeled transport times. The ΔN3 data are the those corrected according to the calibration of a similar CPC for N3 > 3 × 10^5 cm^{-3}. The red lines are the fittings to the data with different estimated transport times. The blue lines are the number concentrations and diameters modeled with Eqs. 2 and 3 by using three different initial number concentrations.

condensation and coagulation to particle growth can therefore be given.

Despite the uncertainties, the observation of particle growth is consistent with other studies on biomass burn smoke plume evolution. For instance, Akagi *et al*. (2012) measured, among several other quantities, refractory black carbon (rBC) concentrations and size distributions with a single particle soot photometer (SP2), light scattering coefficient and CO_2 concentration in a Californian prescribed fire smoke plume. Their measurements showed that the fraction of thickly coated rBC particles of all BC particles and the ratio of excess scattering to excess CO_2 ($\Delta\sigma_{sp}/\Delta CO_2$) increased rapidly within about 20 minutes from emission. They concluded that in the smoke plume, the rBC particles get coated and scatter more light due to size increase and due to the change of the refractive index. Kondo *et al*. (2011) analyzed Asian and North American biomass burn plumes and discussed the role of coagulation and condensation to the observed growth of BC particles. They concluded that during the early stages of BC growth, coagulation may play an important role.

Emission ratios of aerosols with CO_2 as the reference

Trace compound emissions from biomass burning can be expressed as an emission factor (EF) or as an emission ratio (ER) that relates the emission of the compound *X* to that of a reference compound, such as CO or CO_2. If there are several simultaneous ΔX and ΔCO_2 values, the emission ratio can be calculated by fitting the line $\Delta X = ER_{X/CO2}\Delta CO_2$ with a linear regression

with the offset forced to zero (e.g. Yokelson *et al*. 1999, Simpson *et al*. 2011). Here, the emission ratios were studied by calculating the regressions of ΔN3, $\Delta\sigma_{sp}$, $\Delta\sigma_{ap}$ with ΔCO_2 in the plume crossings (Fig. 10). The best relationship was that between $\Delta\sigma_{ap}$ and ΔCO_2 and the second best that between ΔN3 and ΔCO_2. This is expected, since the light absorbing aerosol (BC) is emitted at the same time with CO_2 and dilution is the main mechanism that decreases their concentration, as was discussed above. For the particle number concentration and scattering coefficient, their relation to emissions is expected to be less linear due to other processes affecting their values: particle number decreases also by coagulation and scattering increases by condensational growth.

In order to evaluate the obtained emission factors and ratios, we compared them with other published data. Andreae and Merlet (2001) presented the emission factors of several trace gases and aerosols in grams per kilogram of burned dry biomass in various types of forests. They did not present values for boreal forests, the closest forest type was "extratropical forests." For them they gave the emission factors 1569 ± 131 g kg^{-1} and 0.56 ± 0.19 g kg^{-1} for CO_2 and BC, respectively, and for the number of particles 3.4×10^{15} particles per kg. By using these values it can be estimated that the emission ratios are $BC/CO_2 \approx 0.000357 \pm 0.000152$ (unitless) and $N/CO_2 \approx (2.17 \pm 0.18) \times 10^{12}$ particles per g of CO_2.

The particle number concentration to CO_2 ratio (in cm^{-3} ppm^{-1}) was first calculated from the table in Andreae and Merlet (2001). At 20 °C, 1 ppm of CO_2 equals 1.83 mg m^{-3} and with the ratio of $(2.17 \pm 0.18) \times 10^{12}$ particles per g of CO_2 the estimated number concentration is about (3960 ± 330) cm^{-3} per ppm of CO_2 (Fig. 10a). The mean ratio (± SD) between the particle number concentration and CO_2 in the smoke plume data was (5880 ± 1780) cm^{-3}/ppm of CO_2. The mean is 48% higher than the ratio of 3960 cm^{-3}/ppm of CO_2 derived from the emission factors by Andreae and Merlet (2001). On the other hand, the slope ± SE of the linear regression with the offset forced to zero was (4370 ± 310) cm^{-3}/ppm of CO_2, which is only about 10% higher than the ratio by Andreae and Merlet (2001).

The relationship between $\Delta\sigma_{sp}$ and ΔCO_2 is described better with a power function than with a linear regression (Fig. 10b). By using the linear regression with the offset forced to zero, the squared correlation was negative, which shows that $\Delta X = ER_{X/CO2} \times \Delta CO_2$ is not a valid model

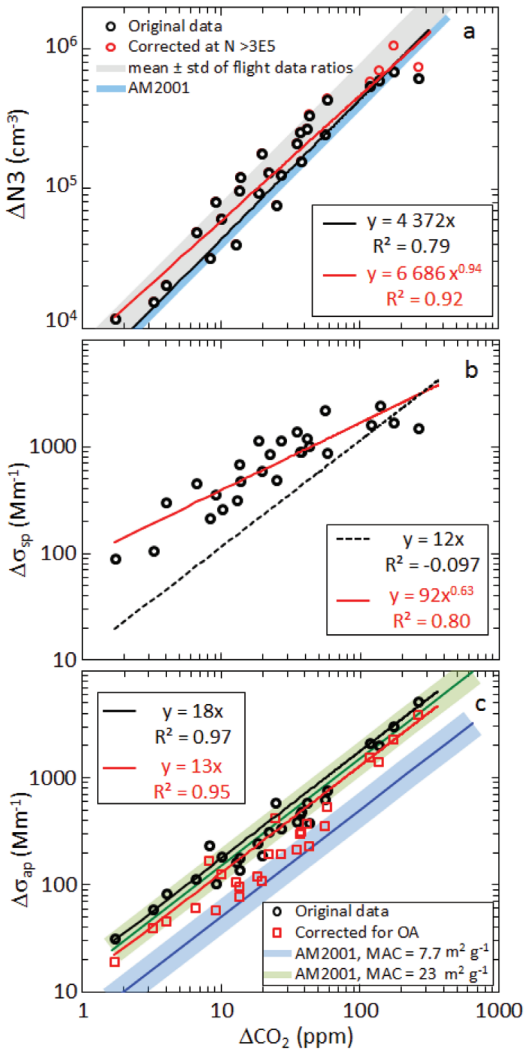

Fig. 10. Relationships between mean excess concentrations: (**a**) number concentrations (ΔN3) with and without using the calibration corrections, (**b**) scattering coefficients ($\Delta\sigma_{sp}$), and (**c**) absorption coefficients ($\Delta\sigma_{ap}$) *vs*. mean excess carbon dioxide (ΔCO_2) concentration in flaming-phase smoke plume crossings. In **c** the black circles: $\Delta\sigma_{ap}$ without additional organic aerosol bias correction, red squares: $\Delta\sigma_{ap}$ calculated with organic aerosol bias correction (Eq. 11). In **a** the fittings were done to the data corrected for the calibrations at $N3 > 3 \times 10^5$ cm^{-3}. In **a** and **c** the blue line denoted by AM2001 presents the ratios and uncertainties calculated from the tables in Andreae and Merlet (2001).

for these data. This is most probably due to the growth of particles both by coagulation and condensation and the increasing scattering per particle as discussed above. This is qualitatively consistent with Akagi *et al*. (2011), who found that the ratio $\Delta\sigma_{sp}/\Delta CO_2$ increased by a factor of 2.5 in a Californian prescribed fire smoke plume over the course of 4 h.

The relation between $\Delta\sigma_{ap}$ and ΔCO_2 was close to linear (Fig. 10c) and can be compared with published data. If CO_2 concentration is 1 ppm and if $BC/CO_2 \approx 0.000357 \pm 0.000152$, as calculated above from the emission factors presented by Andreae and Merlet (2001), the BC concentration is approximately 0.65 ± 0.28 μg m^{-3} and the respective $\sigma_{ap} \approx 5.0 \pm 2.1$ Mm^{-1} with MAC = 7.7 m^2 g^{-1}. So, the σ_{ap}-to-CO_2 ratio is approximately 5.0 ± 2.1 Mm^{-1}/ppm of CO_2 (*see* the blue line in Fig. 10c). The data from the airborne measurements had clearly higher σ_{ap}-to-CO_2 ratios, being approximately 18 ± 1 Mm^{-1}/ppm of CO_2, i.e. higher by a factor of about 3.6. Unless our measured ratio was really higher, there are basically three different possible explanations: (1) The value of MAC = 7.7 m^2 g^{-1} was not applicable to the observed aerosol, (2) the absorption coefficients were overestimated, or (3) the CO_2 concentrations were underestimated. To test the first explanation, the BC-to-CO_2 ratio by Andreae and Merlet (2001) was again used but with MAC multiplied by the factor of 3, so with MAC = 23 m^2 g^{-1} the data agreed with the ratio (Fig. 6c). This MAC is clearly higher than the published ones, so this is not the most probable explanation. The overestimation of absorption is a more probable explanation. The $\Delta\sigma_{ap}$ data corrected additionally according to Eq. 11 were lower (Fig. 10c, red squares), the σ_{ap}-to-CO_2 ratio was approximately 13 ± 1 Mm^{-1}/ppm of CO_2, but still by a factor of about 2.6 higher than calculated from the BC-to-CO_2 ratio by Andreae and Merlet (2001). The underestimation of ΔCO_2 concentrations is still possible after the redistribution method but not likely by a factor of three (*see* the discussion on Fig. 5a.

Emission factor estimates

The emission factors were estimated from Eq. 4 as described above. Here the procedure is followed step by step in Figs. 11–13. The plume cross-section area grew by almost two orders of magnitude from less than 1 ha to about 80 ha when the smoke rose to the height of ~1400 m a.g.l. (Fig. 11a). At the same time, the excess concentrations decreased by almost an order of magnitude (Fig. 11b–d), so that the product of the excess concentrations and the plume cross section area ($\Delta X_i A_i$) did not have a significant trend as a function of height (Fig. 12).

As explained above, in the first method the product ($\Delta X_i A_i$) was extrapolated to the ground level, multiplied by the measured vertical velocity v_{z0} and the flaming phase duration t_F. For example, for CO_2 the extrapolated ($\Delta X_i A_i$) was 206 ± 73 mg m^{-3} ha where the uncertainty is the standard error obtained from the linear regression. With v_{z0} = 4.5 m s^{-1} and t_F = 2 h 15 min = 8100 s, the product yields the total emission of 75 ± 27 tonnes of CO_2. When this is divided by 46.8 tonnes, i.e. the estimated total burned biomass (Virkkula *et al*. 2014), we get an estimated emission factor of 1600 ± 570 g(CO_2) kg^{-1} (burned dry biomass). When the full uncertainties were estimated from Eq. 9, the uncertainty is ±1020 g(CO_2) kg^{-1} (burned dry biomass) (Table 2). The same procedure was used also for the particle number concentrations, POM and BC. For BC the calculation was also repeated including the additional organic aerosol correction (Eq. 11). The emission factors calculated using the measured v_{z0} are presented in column A of Table 2. The emission factors were next estimated by using the vertical velocities obtained from the BUOYANT model. The flux through each plume crossing i was calculated from $\Delta X_i A_i v_{zi}$ and extrapolated to the ground ($\Delta X_0 A_0 v_{z0}$) (Fig. 13). It was then multiplied by t_F = 8100 s to get the emitted mass (column B in Table 2). The concentrations and uncertainties in plume crossings 8 and 26 were very high, so all calculations were repeated by excluding them (the tag "excluding outliers" (EOL) in Table 2). For CO_2 and BC emission factor estimates, the outlier exclusion had a clear reducing effect but negligible for the particle number and POM.

The relative uncertainties $\delta N3/N3$, $\delta\sigma_{sp}/\sigma_{sp}$, $\delta\sigma_{ap}/\sigma_{ap}$, and $\delta CO_2/CO_2$ in Eqs. 6–9 were all set to 0.1, $\delta MSC/MSC = 0.8/3.1 \approx 0.26$, $\delta MAC/MAC$

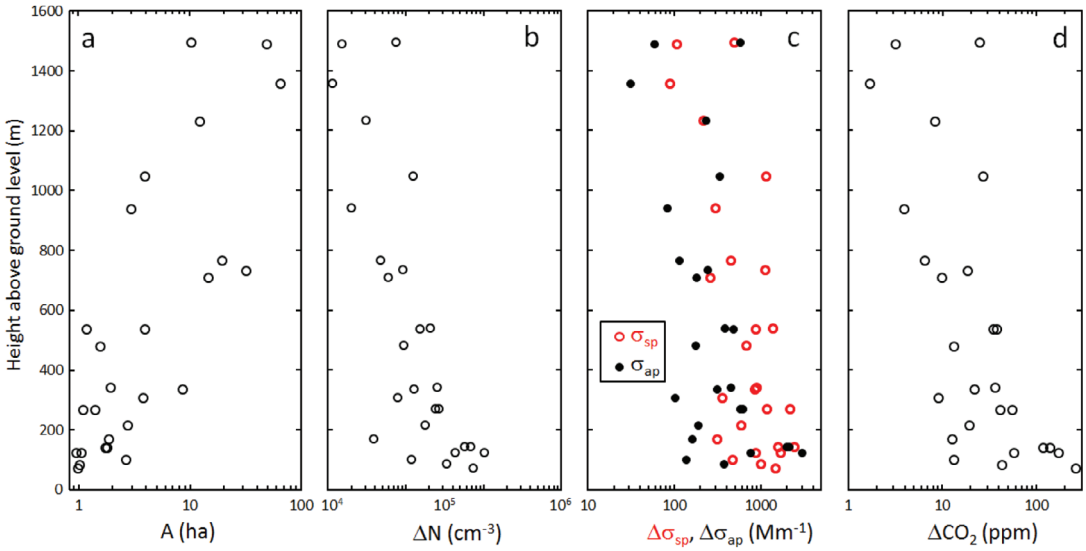

Fig. 11. Flight 1 plume crossing mean concentrations and areas. (**a**) Plume crossing cross section area, (**b**) mean excess particle number concentration (ΔN3), (**c**) mean excess scattering ($\Delta\sigma_{sp}$) and absorption ($\Delta\sigma_{ap}$) coefficients, and (**d**) mean excess carbon dioxide concentration (ΔCO_2) at the heights of the plume crossings.

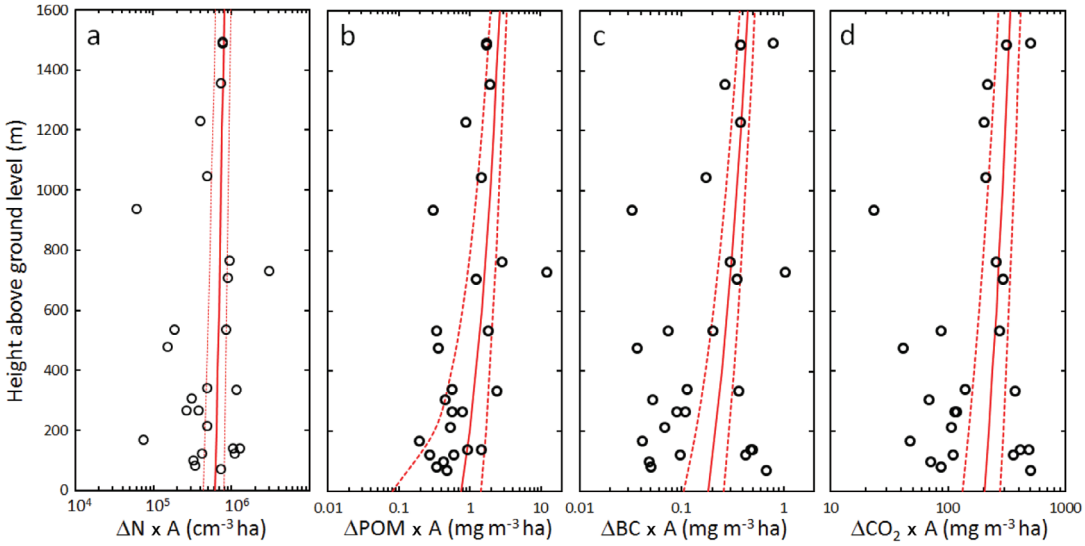

Fig. 12. The product of (**a**) mean ΔN3, (**b**) particulate organic matter (POM), (**c**) black carbon (BC), and (**d**) ΔCO_2 and plume area in each crossing of the plume. The continuous line is the linear fit of $(cA)_z = kz + (cA)_0$ to the data. The dashed lines are calculated by using the same slope k but by using standard errors ($SE_{(cA)0}$) of the offset from the respective fits to get $(cA)_0 \pm SE_{(cA)0}$.

= 1.2/7.7 ≈ 0.16, $\delta m_{BM}/m_{BM}$ = 10 900/46 800 ≈ 0.23, and the uncertainty of vertical velocity $\delta v_z/v_z = 0.2$. The relative uncertainties obtained from the linear regressions ($\delta EF_R/EF_R$) were 0.32, 0.42, 0.91, and 0.54 for N3, CO_2, POM, and BC, respectively, when the regressions were calculated for height vs. the product $\Delta X_i A_i$ and 0.19, 0.23, 0.42, and 0.28, respectively, and when the regressions were calculated for height vs flux $F_i = \Delta X_i A_i v_{zi}$. The uncertainty of the flaming-phase time δt_F was set to 15 min, so $\delta t_F/t_F$ = 900/8100 ≈ 0.11. These relative uncertainties were applied in Eqs. 6–9 to get the uncertainties in the columns A and B of Table 2.

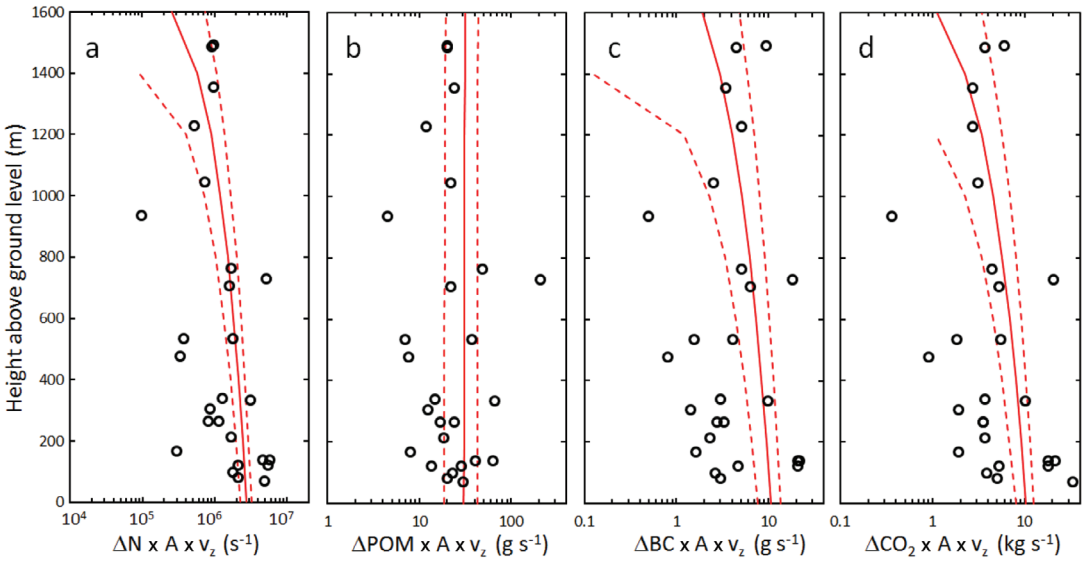

Fig. 13. The flux of particles, POM, BC, and CO_2 through the plume crossings. The continuous line is the linear fit of $(cAv_z)_Z = kz + (cAv_z)_0$ to the data. The dashed lines are calculated by using the same slope k but by using standard errors ($SE_{(cAvz)0}$) of the offset from the respective fits to get $(cA)_0 \pm SE_{(cAvz)0}$.

Table 2. Emission factors (EF) estimated from the airborne measurements and for comparison emission factors presented by Andreae and Merlet (2001) (AM2001) and McMeeking *et al.* (2009). The EFs of CO_2, POM, and BC given as g kg^{-1} of burned dry biomass. The EFs of particle number (*N*) are given as number of particles per kg of burned dry biomass. A: EFs calculated by using the vertical velocities measured at 12 m AGL; B: EFs calculated by using vertical velocities modeled with BUOYANT; ALL: calculations by using all plume crossings; EOL: calculations by excluding outliers, i.e., crossings no. 8 and 26; BC: Black Carbon calculated from the absorption coefficients without additional correctionas; BC_{OACORR}: Black Carbon calculated from absorption coefficients with an additional correction for organic aerosols, Eq. 11.

		This study		AM2001 extratropical forest	McMeeking *et al.* (2009) boreal forest	Unit
		A	B			
CO_2	ALL	1600 ± 1020	1780 ± 960	1569 ± 131	1311 ± 325; 1588 ± 125[b]	g kg^{-1}
	EOL	1280 ± 910	1260 ± 700			
N	ALL	(4.8 ± 2.9) × 10^{15}	(4.8 ± 2.5) × 10^{15}	3.4 × 10^{15}		kg^{-1}
	EOL	(4.4 ± 2.8) × 10^{15}	(4.0 ± 2.2) × 10^{15}			kg^{-1}
POM	ALL	5.9 ± 6.3	5.3 ± 3.7	8.6–9.7[a]	7.8 ± 7.2[c]; 6.2 ± 2.8[d]	g kg^{-1}
	EOL	6.5 ± 7.1	5.3 ± 3.8			g kg^{-1}
BC	ALL	1.4 ± 1.0	1.8 ± 1.1	0.56 ± 0.19	0.2 ± 0.4[e]; 0.60 ± 0.46[f]	g kg^{-1}
	EOL	0.89 ± 0.78	1.3 ± 0.7			g kg^{-1}
BC_{OACORR}	ALL	0.95 ± 0.65	1.1 ± 0.6			g kg^{-1}
	EOL	0.52 ± 0.46	0.71 ± 0.43			g kg^{-1}

[a] emission factor of organic carbon OC from Andreae and Merlet (2001) table 1.
[b] emission factor of CO_2 from black spruce from McMeeking *et al.* (2009) table 2a.
[c] emission factor of OC from boreal forest from McMeeking *et al.* (2009) table 2b.
[d] emission factor of OC from black spruce from McMeeking *et al.* (2009) table 2b.
[e] emission factor of EC from boreal forest from McMeeking *et al.* (2009) table 2b.
[f] emission factor of EC from black spruce from McMeeking *et al.* (2009) table 2b.

For comparison, the emission factors presented by Andreae and Merlet (2001) for extratropical forest fires and the emission factors presented by McMeeking *et al*. (2009) are also shown in Table 2. McMeeking *et al*. (2009) characterized the gas- and speciated aerosol-phase emissions from the open combustion of several plant species in controlled laboratory burns. In those experiments biomass representing boreal forest was also burned. Among others, McMeeking *et al*. (2009) reported the emission factors of elemental and organic carbon (EC and OC) analyzed with thermal-optical methods from quartz filter samples. EC is the dominant light absorber of carbonaceous aerosols but it is not exactly the same as BC that is by definition measured with optical methods. Another point worth noting is that both Andreae and Merlet (2001) and McMeeking *et al*. (2009) report the emission factor of OC, not POM. McMeeking *et al*. (2009) did not report emission factor of particle number.

The results from the present work in Table 2 are in a reasonably good agreement with both Andreae and Merlet (2001) and McMeeking *et al*. (2009), considering all the sources of uncertainty: the concentrations, the areas, the vertical velocity, burning time, and the estimated amount of burned organic material. Another assumption that definitely is not true is that the fire power is constant. This of course is not true and explains some of the scatter of the data. The derived emission factor of particle number is larger than that reported by Andreae and Merlet (2001), but the latter value is within the standard errors of the emission factor in this work. The emission factor of BC is twice as much as that presented by Andreae and Merlet (2001) and three times higher than that presented by McMeeking *et al*. (2009) for boreal forest. A probable reason for this is that a significant amount of absorption by the PSAP was due to the organics condensed onto the filter, as described above. When the estimated effect of condensed organics was removed according to Eq. 11, the emission factors were approximately by a factor of 1.6 ± 0.2 smaller (Table 2). However, even after correcting the absorption data with Eq. 11, the BC emission factors were higher than those in Andreae and Merlet (2001) and McMeeking *et al*. (2009). Yet another possible reason for the differences is that the emission factors reported by McMeeking *et al*. (2009) were based on biomass combustion in a laboratory where the environmental conditions and the actual biomass are different from those in the field. Furthermore, McMeeking *et al*. (2009) reported the emission factor of Elemental Carbon (EC) that was analyzed with thermal-optical methods. Comparisons between BC obtained from filter-based optical methods and EC analyzed with thermal-optical methods showed that the EC concentration may be lower than the BC concentration (e.g. Yelverton *et al*. 2014).

Observations of small particles in the smoldering phase

During flights 2 and 3, the air above the burn area was very different from that observed during the flaming-phase flight: CO_2 concentration did not exceed background levels and both scattering and absorption coefficients exceeded their background values only a few times, and even then not by several orders of magnitude as they did during flight 1 (Fig. 2). Also, particle number concentrations were lower in the later flights. During flight 2, high concentrations of 10^4–10^5 cm^{-3} were measured at several heights up to about 1500 m a.g.l. (Fig. 3a). During flight 3, the highest concentration was ~4×10^4 cm^{-3} at the height of 110 m a.g.l., at 305 m AGL there was one peak concentration of 3400 cm^{-3}, while higher up there were no observations of particles originating from the smoldering ground (Fig. 3), indicating that vertical motion due to convection was much weaker than during the flaming phase. During both smoldering-phase flights, the high concentrations were observed at the horizontal distance of less than 3 km from the center of the burn area (Fig. 3b).

The negligible increase in scattering during flights 2 and 3 suggests that the particles were small. Combining the scattering and number concentration data gives some information of particle sizes. There were several number concentration peaks with the value of N3 in the range of (1–4) $\times 10^4$ cm^{-3}, yet the value of σ_{sp} remaining in the range of 15–20 Mm^{-1} (Fig. 2),

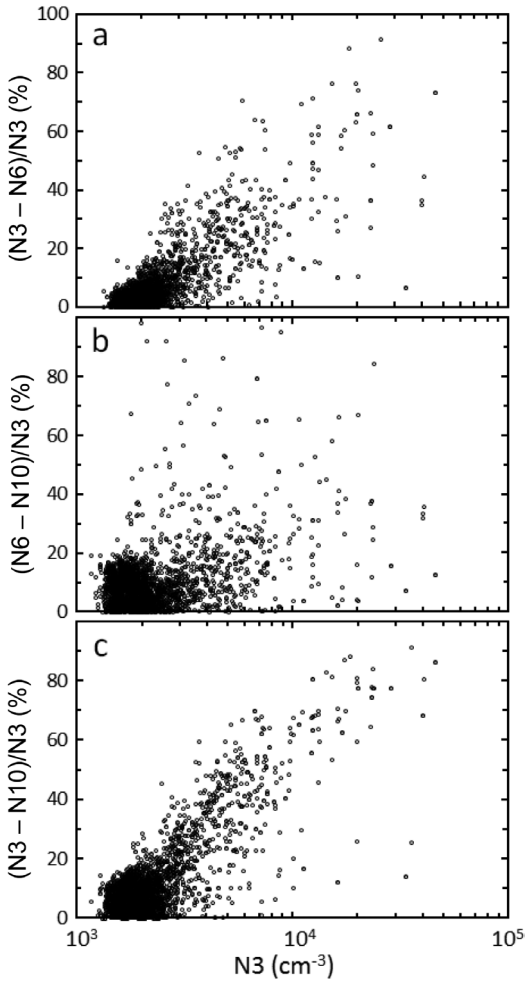

Fig. 14. Fractions of particle number concentrations in the particle diameter range of (**a**) 3–6 nm, (**b**) 6–10 nm, and (**c**) 3–10 nm measured with three condensation particle counters with the cut-off sizes of 3 nm (N3), 6 nm (N6), and 10 nm (N10) as a function of N3 during the smoldering phase flights 2 and 3.

which leads to the value of D_{Csca} in the range of 22–50 nm when calculated using Eq. 1. These values are smaller than the values of D_{Csca} calculated from the flight 1 plume crossing data. It has to be noted also that this D_{Csca} range was calculated from the total scattering coefficients, not from the excess values as in the flight 1 plume crossing analyses. Most excess scattering coefficients in the N3 concentration peaks, during flights 2 and 3, were smaller than 5 Mm^{-1}, so the data suggests that the particles were even smaller than the above-mentioned range. It is not realistic to make any further analyses of the particle size of such small particles with the scattering data, however.

A better indication of the particle size can be obtained from the particle counter data. A simplified size distribution was calculated from the particle number concentrations measured with the particle counters with the size cut-offs of 3, 6 and 10 nm. The fractions of particles in the size ranges of 3–6 nm, 6–10 nm and 3–10 nm were calculated from 100 × (N3–N6)/N3, 100 × (N6–N10)/N3, and 100 × (N3–N10)/N3, respectively. The order of the number concentrations with the size cut-offs of 3, 6 and 10 nm should be N3 ≥ N6 ≥ N10. This was the case in most of the data even at low concentrations, even though this order was more prominent at higher values of N3 (Fig. 14). The data from flights 2 and 3 were classified into three concentration classes: N3 < 3000 cm^{-3}, 3000 < N3 < 10 000 cm^{-3} and N3 > 10 000 cm^{-3}, and simple descriptive statistics were calculated for the size ranges 3–6 nm, 6–10 nm and 3–10 nm (Fig. 15). When N3 < 3000 cm^{-3}, the respective median fractions were –2%, 1%, and 3%, i.e., close to 0%, which means most particles were larger than 10 nm and the counters agreed well. The negative fraction means that the counter with the 6 nm cutoff measured approximately 2% higher concentrations than the counter with the 3 nm cutoff, which is within the uncertainties of the counters. The higher the total concentration was, the larger was the fraction in the size ranges < 10 nm. In the N3 concentration class > 10 000 cm^{-3}, the 75th percentile of the number fraction in the size range 3–10 nm was as high as 78%. In other words, in this concentration class in 25% of the data, more than 78% of particles were smaller than 10 nm. This suggests that there was new particle formation in the air during the smoldering phase, since the primary particles are not expected in the sub-10-nm size range. A possible explanation is that some low-volatile gases emitted from the smoldering ground are the precursors for the particles. No trace gases other than CO_2 were measured during the flights so no hypotheses are presented here.

The low or negligible excess scattering coefficients and indications of particles smaller than 10 nm are in contrast to the observations on

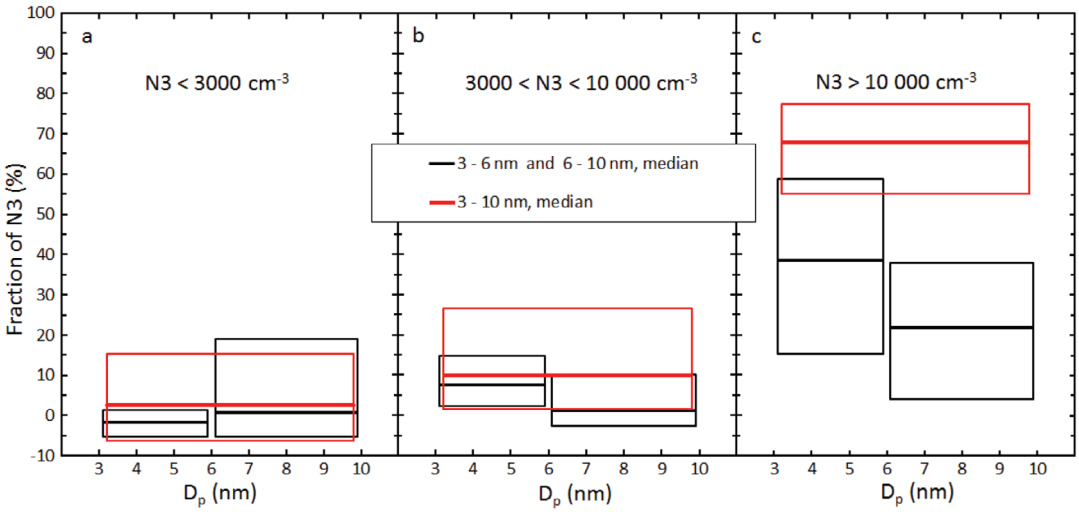

Fig. 15. Median fractions of number concentrations of particles larger than 3 nm (N3) in the size ranges 3–6 nm, 6–10 nm and 3–10 nm in three different particle concentration ranges: (**a**) N3 < 3000 cm^{-3}, (**b**) 3000 < N3 < 10 000 cm^{-3}, and (**c**) N3 > 10 000 cm^{-3} during the smoldering phase, flights 2 and 3. The boxes present the 25th to 75th percentile range of the fractions in the respective size ranges.

ground. The smoke aerosol that was observed at the aerosol cottage at SMEAR II was both larger and more strongly scattering during the smoldering phase than during the flaming phase (Virkkula *et al*. 2014). The differences between airborne and ground-based measurements of fire emissions are not unprecedented, they are in agreement with other studies. Residual smoldering combustion emissions are not influenced by the fire-induced convection and may remain near the ground if there are no winds to loft them higher. As a result, emission factors derived from airborne measurements only underestimate the total fire-integrated emissions (e.g. Bertschi *et al*. 2003, Christian *et al*. 2007, Yokelson *et al*. 2008). The lofted and unlofted emissions from wildfires can also have different chemistry and post-emission transport (e.g. Akagi *et al*. 2011).

Summary and conclusions

Airborne measurements made during a prescribed fire experiment in forest slash fuels in June 2009 were analyzed. There were three flights during the experiment, one during the flaming phase and two during the smoldering phase. During the flaming phase, the smoke plume was flown through at several altitudes and the plume crossing data were analyzed in detail. The plume was so narrow at the lowest altitudes that the aircraft flew through it in about 3 seconds, which corresponds to plume widths of about 120 m. The concentrations and aerosol properties in these plume crossings were analyzed as a function of distance from the burning area and as a function of estimated time of transport since the emission. The latter way of analysis is more general because the processes are time dependent. However, the uncertainties are higher since the locations are obtained directly from the GPS but the transport time was modeled.

The transport times and particle number concentrations in the plume crossings were used for evaluating the role of coagulation in the observed decrease of number concentrations and particle growth. Particle number concentrations decreased from their initial values of about ~$(3 \pm 1) \times 10^6$ cm^{-3} considerably faster than what can be explained by coagulation, which suggests that dilution was the main mechanism leading to the decrease in the particle number concentration. There were also some indications of particle growth during the transport from the burn area, but since particle size distributions were not measured on board the aircraft, it is not possible to get exact information on this phenom-

enon. However, the effective scattering cross section diameter, D_{Csca}, calculated from the ratio of scattering coefficient and particle number concentration increased from about 50 nm to 100 nm during the first 1000 m of transport from emission. The increase of D_{Csca} was faster than what can be explained by coagulation, which suggests that condensation played an important role in growing the particles even at the early stages of the smoke plume. Another indication of the particle growth was the increase of the particle single-scattering albedo: this quantity increased from about 0.4 ± 0.1 at the nearest plume crossings to about 0.8 ± 0.1 at a distance of about 400 m from the burning area, consistent with the values measured at the ground-based SMEAR II station. However, it is possible that the single-scattering albedo was higher than 0.4 ± 0.1 even at the lowest levels. The reason is that in the fastest plume crossings the scattering coefficient may have been underestimated due to too slow response time of the nephelometer.

The mean Ångström exponent of absorption was 1.70 ± 0.24 in the smoke plume crossings, which is in line with published spectral absorption of wood smoke filter samples. There was a positive relation between the single-scattering albedo and Ångström exponent of absorption. The latter was calculated from the absorption coefficients that were not corrected for scattering, which suggests that the low single-scattering albedos were not only due to underestimated scattering.

The amount of CO_2 and black carbon and number and mass of particles emitted during the experiment were estimated by combining information from the airborne measurements and vertical flow velocity measured near the surface within the burning area and vertical velocities modeled with a plume rise model. The estimated emission factors were 1600 ± 1020, 5.9 ± 6.3 and 1.4 ± 1.0 g kg^{-1} (dry biomass), for CO_2, particulate organic matter and black carbon, respectively, and $(4.8 \pm 2.9) \times 10^{15}$ particles per kg (dry biomass) for particles larger than 3 nm in diameter. The uncertainties associated with these emission factors are high, as was shown in a sensitivity test in which two plume crossings with the highest and most uncertain concentrations were excluded from the calculations. It has to be noted, though, that the emissions of both aerosols and CO_2 were calculated only from the flaming phase data, so the whole fire-integrated emissions were underestimated. The obtained emission factors were not significantly different from those presented in the literature, with the exception of that for black carbon. However, the absorption coefficient and thus the black carbon concentration may have been overestimated by a factor of about 1.6 ± 0.2 due to condensation of organics on the filter of the absorption photometer. This leads to an overestimation of the black carbon emission factor estimate.

The data suggest that particles originating from residual smoldering combustion can be observed without elevated CO_2 concentrations. Contrary to the flaming-phase flight, during the smoldering phase flights there were no excess CO_2 concentrations and both scattering and absorption coefficients exceeded their background values only slightly. This is different from the scattering coefficients recorded on the ground where the aerosol was more strongly scattering during the smoldering phase than during the flaming phase. This difference suggests that the particles observed aloft during the smoldering phase were much smaller than at the ground level.

Simplified size distributions were calculated from the data of three CPCs with different cut-offs. They showed that when particle number concentrations exceeded 10 000 cm^{-3} the majority of particles were smaller than 10 nm in diameter, suggesting that new particles were formed. Sub-10-nm particles are not climatically significant because they do not scatter enough light to contribute to the direct radiative forcing, and because they are too small to be able to act as cloud condensation nuclei (CCN). They may, however, become CCN after their growth to larger sizes in case condensable compounds are available. The residual smoldering combustion is a potentially a important source of particles as it may continue for days after the flaming combustion has ended. However, the data obtained here are too few to make any quantitative estimate of the emission factors related to the smoldering phase. To confirm the observations of new particle formation, measurements should be conducted over smoldering fires with instruments

that can measure size distributions starting from diameters smaller than 10 nm.

Acknowledgements: The project was supported by the Academy of Finland as part or the Centre of Excellence program (project no. 1118615) and as part of the IS4FIRES project (decision no. 122870), by the Nordic Centre of Excellence CRAICC (CRyosphere-Atmosphere Interactions in Changing Climate), TEKES (project KASTU, decision no. 40208/08 and KASTU-2, decision no. 40393/10), by the European Commission 6th framework program project (EUCAARI), contract 036833-2, European Union Seventh Framework Programme (FP7/2007–2013) under grant agreement no. 262254 (ACTRIS), University of Helsinki, Finnish Meteorological Institute, and San José State University, CA, USA.

References

Akagi S.K., Yokelson R.J., Wiedinmyer C., Alvarado M.J., Reid J.S., Karl T., Crounse J.D. & Wennberg P.O. 2011. Emission factors from open and domestic biomass burning for use in atmospheric models. *Atmos. Chem. Phys.* 11: 4039–4072.

Akagi S.K., Craven J.S., Taylor J.W., McMeeking G.R., Yokelson R.J., Burling I.R., Urbanski S.P., Wold C.E., Seinfeld J.H., Coe H., Alvarado M.J. & Weise D.R. 2012. Evolution of trace gases and particles emitted by a chaparral fire in California. *Atmos. Chem. Phys.* 12: 1397–1421.

AMAP 2011. *The impact of black carbon on Arctic climate*. Arctic Monitoring and Assessment Programme (AMAP), Oslo.

Andreae M. & Merlet P. 2001. Emission of trace gases and aerosols from biomass burning. *Glob. Biogeochem. Cycles* 15: 955–966.

Bertschi I., Yokelson R.J., Ward D.E., Babbitt R.E., Susott R.A., Goode J.G. & Hao W.M. 2003. Trace gas and particle emissions from fires in large diameter and belowground biomass fuels. *J. Geophys. Res.* 108(D13), 8472, doi:10.1029/2002JD002100.

Bond T.B. & Bergstrom R.W. 2006: Light absorption by carbonaceous particles: an investigative review. *Aerosol Sci. Technol.* 40: 27–67.

Bond T.C., Doherty S.J., Fahey D.W., Forster P.M., Berntsen T., DeAngelo B.J., Flanner M.G., Ghan S., Kärcher B., Koch D., Kinne S., Kondo Y., Quinn P.K., Sarofim M.C., Schultz M.G., Schulz M., Venkataraman C., Zhang H., Zhang S., Bellouin N., Guttikunda S.K., Hopke P.K., Jacobson M.Z., Kaiser J.W., Klimont Z., Lohmann U., Schwarz J.P., Shindell D., Storelvmo T., Warren S.G. & Zender C.S. 2013: Bounding the role of black carbon in the climate system: a scientific assessment. *J. Geophys. Res.* 118: 5380–5552, doi:10.1002/jgrd.50171.

Burling I.R., Yokelson R.J., Akagi S.K., Urbanski S.P., Wold C.E., Griffith D.W.T., Johnson T.J., Reardon J. & Weise D.R. 2011. Airborne and ground-based measurements of the trace gases and particles emitted by biomas. *Atmos. Chem. Phys.* 11: 12197–12216.

Cappa C., Lack D., Burkholder J. & Ravishankara A. 2008. Bias in filter based aerosol light absorption measurements due to organic aerosol loading: rvidence from laboratory measurements. *Aerosol Sci. Technol.* 42: 1022–1032.

Carrico C.M., Petters M.D., Kreidenweis S.M., Sullivan A.P., McMeeking G.R., Levin E.J.T., Engling G., Malm W.C. & Collett J.L. 2010. Water uptake and chemical composition of fresh aerosols generated in open burning of biomass. *Atmos. Chem. Phys.* 10: 5165–5178.

Chand D., Wood R., Anderson T.L., Satheesh S.K. & Charlson R.J. 2009. Satellite-derived direct radiative effect of aerosols dependent on cloud cover. *Nature Geosci.* 2: 181–184.

Cross E.S., Onasch T.B., Ahern A., Wrobel W., Slowik J., Olfert J., Lack D., Massoli P., Cappa C., Schwarz J., Spackman R., Fahey D., Sedlacek A., Trimborn A., Jayne J., Freedman A., Williams L., Ng N.L., Mazzoleni C., Dubey M., Brem B., Kok G., Subramanian R., Freitag S., Clarke A., Thornhill D., Marr L., Kolb C., Worsnop D. & Davidovits P. 2010. Soot particle studies — instrument inter-comparison — project overview. *Aerosol Sci. Technol.* 44: 592–611.

Flannigan M.D. & Haar T.V. 1986. Forest fire monitoring using NOAA satellite AVHRR. *Can. J. For. Res.* 16: 975–982.

French N.H., Kasischke E.S., Hall R.J., Murphy K.A., Verbyla D.L., Hoy E.E. & Allen J.L. 2008. Using Landsat data to assess fire and burn severity in the North American boreal forest region: an overview and summary of results. *International Journal of Wildland Fire* 17: 443–462.

Goldammer J.G. & Furyaev V.V. 1996. Fire in ecosystems of boreal Eurasia: ecological impacts and links to the global system. In: Goldammer J.G. & Furyaev V.V. (eds.), *Fire in ecosystems of boreal Eurasia*, Kluwer Acad. Press, Norwell, MA., pp. 1–20.

Hand J.L. & Malm W.C. 2007. Review of aerosol mass scattering efficiencies from ground-based measurements since 1990. *J. Geophys. Res.* 112, D16203, doi:10.1029/2007JD008484.

Hari P. & Kulmala M. 2005. Station for measuring ecosystem-atmosphere relations (SMEAR II). *Boreal Env. Res.* 10: 315–322.

Hinds W.C. 1999. *Aerosol technology*, 2nd ed. John Wiley & Sons, New York.

Hinds W.C. 2001. Physical and chemical changes in the particulate phase. In: Baron P.A. & Willeke K. (eds.), *Aerosol measurement: principles, techniques, and applications*, John Wiley & Sons, New York.

Janhäll S., Andreae M.O. & Pöschl U. 2010. Biomass burning aerosol emissions from vegetation fires: particle number and mass emission factors and size distributions. *Atmos. Chem. Phys.* 10: 1427–1439.

Kaufman Y.J., Remer L.A., Ottmar R.D., Ward D.E., Li R.R., Kleidman R., Fraser R.S., Flynn L., McDougal D. & Shelton G. 1996. Relationship between remotely sensed fire intensity and rate of emission of smoke: SCAR-C

experiment. In: Levine J.S. (ed.), *Biomass burning and global Change*, MIT Press, Cambridge, MA.

Kirchstetter T.W., Novakov T. & Hobbs P.V. 2004. Evidence that the spectral dependence of light absorption by aerosols is affected by organic carbon. *J. Geophys. Res.* 109, D21208, doi:10.1029/2004JD004999.

Kirchstetter T.W. & Thatcher T.L. 2012. Contribution of organic carbon to wood smoke particulate matter absorption of solar radiation. *Atmos. Chem. Phys.* 12: 6067–6072.

Kukkonen J., Nikmo J., Sofiev M., Riikonen K., Petäjä T., Virkkula A., Levula J., Schobesberger S. & Webber D.M. 2014. Applicability of an integrated plume rise model for the dispersion from wild-land fires. *Geosci. Model Dev. Discuss.* 7: 483–527.

Lack D.A., Cappa C.D., Baynard T., Massoli P., Covert D.S., Sierau B., Bates T.S., Quinn P.K., Lovejoy E.R. & Ravishankara A.R. 2008. Bias in filter-based aerosol absorption measurements due to organic aerosol loading: evidence from ambient measurements. *Aerosol Sci. Technol.* 42: 1033–1041.

Law K.S. & Stohl A. 2007. Arctic air pollution: origins and impacts. *Science* 315: 1537–1540.

Lentile L.B., Holden Z.A., Smith A.M., Falkowski M.J., Hudak A.T., Morgan P., Lewis S.A., Gessler P.E. & Benson N.C. 2006. Remote sensing techniques to assess active fire characteristics and post-fire effects. *International Journal of Wildland Fire* 15: 319–345.

Lewis K., Arnott W.P., Moosmüller H. & Wold C.E. 2008. Strong spectral variation of biomass smoke light absorption and single scattering albedo observed with a novel dual-wavelength photoacoustic instrument. *J. Geophys. Res.* 113, D16203, doi:10.1029/2007JD009699.

Mazurek M.A., Cofer W.R. & Levine J.S. 1991. Carbonaceous aerosols from prescribed burning of a boreal forest ecosystem. In: Levine J.S. (ed.), *Global biomass burning*, MIT Press, Cambridge, MA, pp. 258–263.

McMeeking G.R., Kreidenweis S.M., Baker S., Carrico C.M., Chow J.C., Collet J.L.Jr., Hao W.M., Holden A.S., Kirchstetter T.W., Malm W.C., Moosmüller H., Sullivan A.P. & Wold C.E. 2009. Emissions of trace gases and aerosols during the open combustion of biomass in the laboratory. *J. Geophys. Res.* 114, D19210, doi:10.1029/2009JD011836.

McNaughton C.S., Thornhill L., Clarke A.D., Howell S.G., Pinkerton M., Anderson B., Winstead E., Hudgins C., Maring H., Dibb J.E. & Scheuer E. 2007: Results from the DC-8 Inlet Characterization Experiment (DICE): airborne versus surface sampling of mineral dust and sea salt aerosols. *Aerosol Sci. Technol.* 41: 136–159.

Mikhailov E., Vlasenko S., Podgorny I., Ramanathan V. & Corrigan C. 2006. Optical properties of soot-water drop agglomerates: An experimental study. *J. Geophys. Res.* 111: 1–16.

Ogren J. 2010. Comment on "Calibration and Intercomparison of Filter-Based Measurements of Visible Light Absorption by Aerosols". *Aerosol Sci. Technol.* 44: 589–591.

Pratt K.A., Murphy S.M., Subramanian R., DeMott P.J., Kok G.L., Campos T., Rogers D.C., Prenni A.J., Heymsfield A.J. Seinfeld J.H. & Prather K.A. 2011. Flight-based chemical characterization of biomass burning aerosols within two prescribed burn smoke plumes. *Atmos. Chem. Phys.* 11: 12549–12565.

Quinn P.K., Bates T.S., Baum E., Doubleday N., Fiore A.M., Flanner M., Fridlind A., Garrett T.J., Koch D., Menon S., Shindell D., Stohl A. & Warren S.G. 2008. Short-lived pollutants in the Arctic: their climate impact and possible mitigation strategies. *Atmos. Chem. Phys.* 8: 1723–1735.

Randerson J.T., Liu H., Flanner M.G., Chambers S.D., Jin Y., Hess P.G., Pfister G., Mack M.C., Treseder K.K., Welp L.R., Chapin F.S., Harden J.W., Goulden M.L., Lyons E., Neff J.C., Schuur E.A.G. & Zender C.S. 2006. The impact of boreal forest fire on climate warming. *Science* 314: 1130–1132.

Reid J.S., Koppmann R., Eck T.F. & Eleuterio D.P. 2005a. A review of biomass burning emissions part II: intensive physical properties of biomass burning particles. *Atmos. Chem. Phys.* 5: 799–825.

Reid J.S., Eck T.F., Christopher S.A., Koppmann R., Dubovik O., Eleuterio D.P., Holben B.N., Reid E.A. & Zhang J. 2005b. A review of biomass burning emissions part III: intensive optical properties of biomass burning particles. *Atmos. Chem. Phys.* 5: 827–849.

Schnaiter M., Horvath H., Mohler O., Naumann K.H., Saathoff H. & Schock O.W. 2003. UV-VIS-NIR spectral optical properties of soot and soot-containing aerosols. *J. Aerosol Sci.* 34: 1421–1444.

Schnaiter M., Gimmler M., Llamas I., Linke C., Jäger C. & Mutschke H. 2006. Strong spectral dependence of light absorption by organic carbon particles formed by propane combustion. *Atmos. Chem. Phys.* 6: 2981–2990.

Schobesberger S., Väänänen R., Leino K., Virkkula A., Backman J., Pohja T., Siivola E., Franchin A., Mikkilä J., Paramonov M., Aalto P.P., Krejci R., Petäjä T. & Kulmala M. 2013. Airborne measurements over the boreal forest of southern Finland during new particle formation events in 2009 and 2010. *Boreal Env. Res.* 18: 145–163.

Simpson I.J., Akagi S.K., Barletta B., Blake N.J., Choi Y., Diskin G.S., Fried A., Fuelberg H.E., Meinardi S., Rowland F.S., Vay S.A., Weinheimer A.J., Wennberg P.O., Wiebring P., Wisthaler A., Yang M., Yokelson R.J. & Blake D.R. 2011. Boreal forest fire emissions in fresh Canadian smoke plumes: C_1–C_{10} volatile organic compounds (VOCs), CO_2, CO, NO_2, NO, HCN and CH_3CN. *Atmos. Chem. Phys.* 11: 6445–6463.

Stith J.L., Radke L.F. & Hobbs P.V. 1981. Particle emissions and the production of ozone and nitrogen oxides from the burning of forest slash. *Atmos. Environ.* 15: 73–82.

Van de Hulst H.C. 1957. *Light scattering by small particles*. Wiley, New York.

van der Werf G.R., Randerson J.T., Giglio L., Collatz G.J., Mu M., Kasibhatla P.S., Morton D.C., DeFries R.S., Jin Y. & van Leeuwen T.T. 2010. Global fire emissions and the contribution of deforestation, savanna, forest, agricultural, and peat fires (1997–2009). *Atmos. Chem. Phys.* 10: 11707–11735.

Virkkula A. 2010. Correction of the calibration of the 3-wavelength Particle Soot Absorption Photometer (3λ PSAP). *Aerosol Sci. Technol.* 44: 706–712.

Virkkula A., Ahlquist N.C., Covert D.S., Arnott W.P., Sheridan P.J., Quinn P.K. & Coffman D.J. 2005. Modification, calibration and a field test of an instrument for measuring light absorption by particles. *Aerosol Sci. Technol.* 39: 68–83.

Virkkula A., Backman J., Aalto P. P., Hulkkonen M., Riuttanen L., Nieminen T., Dal Maso M., Sogacheva L., De Leeuw G. & Kulmala M. 2011. Seasonal cycle, size dependencies, and source analyses of aerosol optical properties at the SMEAR II measurement station in Hyytiälä, Finland. *Atmos. Chem. Phys.* 11: 4445–4468.

Virkkula A., Levula J., Pohja T., Aalto P.P., Keronen P., Schobesberger S., Clements C.B., Pirjola L., Kieloaho A.-J., Kulmala L., Aaltonen H., Patokoski J., Pumpanen J., Rinne J., Ruuskanen T., Pihlatie M., Manninen H.E., Aaltonen V., Junninen H., Petäjä T., Backman J., Dal Maso M., Nieminen T., Olsson T., Grönholm T., Kerminen V.-M., Schultz D.M., Kukkonen J., Sofiev M., de Leeuw G., Bäck J., Hari P. & Kulmala M. 2014. Prescribed burning of logging slash in the boreal forest of Finland: emissions and effects on meteorological quantities and soil properties. *Atmos. Chem. Phys.* 14: 4473–4502.

Wade D.D. & Lunsford J.D. 1989. *A guide for prescribed fire in southern forests*. R8-TP-11, USDA For. Serv. Tech. Publ.,Washington, DC.

Yelverton T.L.B., Hays M.D., Gullet B.K. & Linak W.P. 2014. Black carbon measurements of flame-generated soot as determined by optical, thermal-optical, direct absorption, and laser incandescence methods. *Env. Eng. Sci.* 31: 209–215.

Yokelson R.J., Goode J.G., Ward D.E., Susott R.A., Babbitt R.E., Wade D.D., Bertschi I., Griffith D.W.T. & Hao W.M. 1999. Emissions of formaldehyde, acetic acid, methanol, and other trace gases from biomass fires in North Carolina measured by airborne Fourier transform infrared spectroscopy. *J. Geophys. Res.* 104: 30109–30125.

Yokelson R.J., Christian T.J., Karl T.G. & Guenther A. 2008. The tropical forest and fire emissions experiment: laboratory fire measurements and synthesis of campaign data. *Atmos. Chem. Phys.* 8: 3509–3527.

Yokelson R.J., Burling I.R., Gilman J.B., Warneke C., Stockwell C.E., de Gouw J., Akagi S.K., Urbanski S.P., Veres P., Roberts J.M., Kuster W.C., Reardon J., Griffith D.W.T., Johnson T.J., Hosseini S., Miller J.W., Cocker D.R.III, Jung H. & Weise D.R. 2013. Coupling field and laboratory measurements to estimate the emission factors of identified and unidentified trace gases for prescribed fires. *Atmos. Chem. Phys.* 13: 89–116.